Published in final edited form as:

Am J Respir Cell Mol Biol. 2004 October ; 31(4): 382–394. doi:10.1165/rcmb.2004-0060OC.

Mucin Is Produced by Clara Cells in the Proximal Airways of Antigen Challenged Mice

Christopher M. Evans[1,3], **Olatunji W. Williams**[1], **Michael J. Tuvim**[1], **Rupesh Nigam**[1], **George P. Mixides**[1], **Michael R. Blackburn**[4], **Francesco J. DeMayo**[2], **Alan R. Burns**[1], **Charlotte Smith**[5], **Susan D. Reynolds**[5], **Barry R. Stripp**[5], **Burton F. Dickey**[3]

[1]Department of Medicine, Baylor College of Medicine, University of Texas Health Science Center, Houston, Texas.

[2]Department of Molecular and Cellular Biology, Baylor College of Medicine, University of Texas Health Science Center, Houston, Texas.

[3]Department of Pulmonary Medicine, MD Anderson Cancer, University of Texas Health Science Center, Houston, Texas.

[4]Department of Biochemistry and Molecular Biology, University of Texas Health Science Center, Houston, Texas.

[5]Department of Environmental and Occupational Health, University of Pittsburgh Graduate School of Public Health, Pittsburgh, Pennsylvania

Abstract

Airway mucus hypersecretion is a prominent feature of many obstructive lung diseases. We thus determined the ontogeny and exocytic phenotype of mouse airway mucous cells. In naïve mice, ciliated (~40%) and non-ciliated (~60%) epithelial cells line the airways, and >95% of the non-ciliated cells are Clara cells that contain Clara cell secretory protein (CCSP). Mucous cells comprise <5% of the non-ciliated cells. After sensitization and a single aerosol antigen challenge, alcian blue-periodic acid Schiff's positive mucous cell numbers increase dramatically, appearing 6 h after challenge (21% of non-ciliated/non-basal cells), peaking from days 1–7 (99%), and persisting at day 28 (65%). Throughout the induction and resolution of mucous metaplasia, ciliated and Clara cell numbers identified immunohisotchemically change only slightly. Intracellular mucin content peaks at day 7, and mucin expression is limited specifically to a Clara cell subset in airway generations 2–4 that continue to express CCSP. Functionally, Clara cells are secretory cells that express the regulated exocytic marker Rab3D and, in antigen challenged mice, rapidly secrete mucin in response to inhaled ATP in a dose dependent manner. Thus, Clara cells show great plasticity in structure and secretory products, yet have molecular and functional continuity in their identity as specialized apical secretory cells.

Corresponding Author: Christopher M. Evans, Ph.D., Pulmonary Medicine, MD Anderson Cancer Ctr., 2121 West Holcombe Blvd., Houston, TX 77030, (713) 563-0403, (713) 563-0411 [FAX], cevans@mdanderson.org.

Introduction

Mucus hypersecretion is a prominent feature of obstructive lung pathologies that, despite long recognition of its contributions to disease morbidities, is not yet sufficiently understood to treat directly. In cystic fibrosis (CF), chronic obstructive pulmonary disease (COPD), and fatal asthma, mucus plugs occlude small airways (1–4). In CF and COPD, excess mucus in the airways contributes to disease morbidity by increasing the frequency and severity of pulmonary infections (5;6) and the severity of airflow obstruction (7;8). The airways of healthy individuals contain few mucous cells, but the airways of humans with asthma and of animals in induced models of asthma display dramatically increased numbers of mucin-producing goblet cells. This trait is commonly referred to as mucous (or goblet) cell metaplasia based on histopathologic criteria. While many of the immunologic and pharmacologic signal transduction pathways involved in the development of this phenotype have been characterized (9–11), there is a paucity of information regarding the cellular and molecular basis of mucous cell differentiation and function. Such information is crucial for understanding the specific mechanisms of mucus overproduction and hypersecretion in obstructive airway diseases.

In the lungs of mice and humans, the airways are lined by a mixed population of ciliated and non-ciliated epithelial cells. In mice, the non-ciliated cells comprise 50–70% of the total epithelial population throughout the entire conducting airway network (12). In naïve mice, the majority of these non-ciliated cells are Clara cells, and there are few or no mucous cells in airways distal to the trachea. In healthy humans, there are few Clara cells in the large conducting airways, but their numbers progressively increase in more distal airways (13;14). Clara cells express and secrete Clara cell secretory protein (CCSP), which is the major component of their secretory granules (15;16). The appearance of granular mucous cells in the airways is a common feature of lung inflammation. Exposure of the lungs to allergic, infectious, or irritant stimuli, however, causes a striking increase in the numbers of mucin-producing cells in both mice and humans. In antigen challenged animals, this process is critically dependent on interleukin (IL)-13 (9;10) and epidermal growth factor (EGF; ref. 11) signaling. Thus, allergic airway inflammation induces the synthesis and storage of mucins, such as Muc5ac, by the airway epithelium (17). However, the cellular origin of mucous cells and the molecular mechansims of mucin release into the airway lumen are not well understood.

Exocytosis is a highly conserved phenomenon in eukaryotic cells that requires the fusion of the lipid bilayer membranes of secretory vesicles and the plasma membrane. This energetically unfavorable process is mediated by the concerted action of a large number of proteins involved in the transport (18), tethering, docking, and fusion of secretory vesicles to the plasma membrane. SNARE proteins are central mediators of vesicle docking and fusion, and their interactions are regulated by members of the Rab GTPase family (19;20). Individual Rab proteins are highly specific for distinct steps of interorganellar vesicle transport and thus serve as selective molecular markers for identifying specific cell trafficking modalities. Two distinct pathways for the apical secretion of newly synthesized proteins in epithelial cells exist. The first, a ubiquitous constitutive pathway, is important for the insertion of newly synthesized membrane proteins and for the secretion of cytokines

and chemokines. Secretion by the constitutive pathway is identified by the localization of Rab8 to secretory vesicles. A second pathway, the regulated exocytic pathway, exists in specialized cells capable of storing newly synthesized proteins in secretory granules for subsequent exocytosis in response to external stimuli. The regulated exocytic pathway is characterized by the localization of Rab3 isoforms on exocytic granules (19;20). Thus, association of these components of the exocytic machinery with secretory compartments of airway epithelial cells is indicative of the precise secretory pathway.

In order to define the cellular mechanisms for the overproduction and secretion of mucus in the lungs *in vivo*, we have assessed the changes in cell types, secretory products, and exocytic proteins of the airway epithelium in antigen challenged mice. We demonstrate on both anatomical and molecular levels the origin of mucous cells as well as their specific exocytic function in the lungs *in vivo*. By clarifying the ontogeny and functional characteristics of mucous cells in mice, our studies provide a framework that may be useful in the future for cell specific therapies in humans and for precisely modeling airway diseases in mice.

Methods

Animals:

Female, specific pathogen free, 4–6 week old BALB/c mice were purchased from Harlan (Indiananpolis, IN). Mice were housed in accordance with the Institutional Animal Care and Use Committee of the Baylor College of Medicine and Houston VA Medical Center. For antigen challenge experiments, mice were sensitized to ovalbumin (20 μg ovalbumin Grade V, 2.25 mg alum in saline, pH7.4, Sigma, St. Louis, MO) administered by intraperitoneal (i.p.) injection) four times, weekly. Sensitized mice were exposed for 30 min to an aerosol of either 0.9% (w/v) saline or 2.5% (w/v) ovalbumin in 0.9% saline, which were both supplemented with 0.02% (v/v) antifoam A silicon polymer (Sigma), via an AeroMist CA-209 compressed gas nebulizer (CIS-US, Inc. Bedford, MA) in the presence of room air supplemented with 5% CO_2 to promote maximal ventilation and homogeneous aerosol exposure throughout the lungs (21). In preliminary studies, we determined that there were no obvious histological differences in the airways between animals challenged singly on day 0 and animals challenged three times on days 0, 1, and 2 (data not shown, n=6). Thus, a single antigen challenge was used in these studies to maximize the precision of measured changes in epithelial cell phenotype at early timepoints and to allow for comparison with later timepoints. The aerosol particles generated were measured using an Andersen cascade impacter (Andersen Instruments, Atlanta, GA) and ranged in sizes from <0.4 μm to 4.7 μm with a mass median aerodynamic diameter of 1.49 μm and a geometric standard deviation of 1.91. The aerosol concentration, measured using an All-Glass Impinger (Ace Glass, Inc., Vineland, NJ), was approximately 350 μg ovalbumin/l air. Based on previous measurements of ventilation and aerosol deposition using this system (22), the calculated total dose of antigen deposited in the lungs was 78.8 μg/animal with an alveolar dose of 26.3 μg/animal (23). Aerosol deposition throughout the airways was confirmed in a small number of mice that received an aerosol of filtered Coomassie brilliant blue R250 solution (0.2%

w/v, 30 min). Dye deposition was observed in the terminal bronchioles using a dissecting microscope (data not shown).

At 6 h and 1, 2, 3, 7, 14, 21, 28, and 90 days following antigen challenge, animals were anesthetized by i.p. injection of a mixture of ketamine, xylazine, and acepromazine. Under deep anesthesia, animals were tracheostomized using a 20 gauge blunt tip cannula and euthanized by exsanguination via the abdominal aorta. In order to assess adequate allergic sensitization and challenge, bronchoalveolar lavage was performed in saline challenged and antigen challenged mice by instilling 2 × 1.0 ml of 0.9% saline via the tracheal cannula. Cells were counted using a hemacytometer (Hauser Scientific, Horsham, PA), cytospun onto glass slides, and stained with Wright-Geimsa. In antigen sensitized, saline challenged mice $1.1 \pm 0.1 \times 10^5$ cells were recovered, and 1.1×10^3 (<1%) were eosinophils (n=5). Three days following antigen challenge, $17.2 \pm 2.8 \times 10^5$ cells were recovered, and 8.8×10^5 (>50%) were eosinophils (n=7). This 800-fold increase in eosinophil number confirmed that the sensitization regimen used in these studies was adequate to produce a robust allergic lung response to a single aerosol challenge.

Histochemistry:

For light microscopic studies, lungs were perfused with saline via the right cardiac ventricle to clear blood from the pulmonary tissues. Fixative (4% paraformaldehyde in 0.1 M phosphate buffer pH 7.0) was infused intratracheally at 10–15 cm pressure. The lungs were fixed *in situ* for 30 min at room temperature, removed from the thoracic cavity, and fixed overnight at 4°C. Lungs were embedded in paraffin and cut into 6 μm sections longitudinally along the dorsal aspect to reveal the length of the main axial bronchus and minor daughter branches of one or more lung lobes.

Hematoxylin and eosin staining was performed by incubating the tissues in Weigert's iron hematoxylin followed by serial eosin and graded ethanol steps. Mucin glycoconjugates were stained using 1% Alcian blue (pH 2.5) and periodic acid Schiff (AB-PAS) with a methyl green counterstain for brightfield light microscopy as follows. Tissues were first oxidized in 1% periodic acid (10 min), rinsed, and treated with Schiff's reagent (0.5% pararosaniline w/v, 1% sodium metabisulfite w/v, 0.01 N HCl) for 15 min then dehydrated in ethanol and xylene and permanently mounted with cytoseal 60 (Fisher Chemicals, Fairlane, NJ). For fluorescent labeling of mucin, tissues were stained using a periodic acid fluorescent Schiff (PAFS) staining procedure in which acriflavine was substituted for pararosaniline. For PAFS labeling, tissues were oxidized as above, rinsed, treated with acriflavine fluorescent Schiff's reagent (0.5% acriflavine w/v, 1% sodium metabisulfite w/v, 0.01 N HCl) for 20 min, rinsed in ddH_2O, and rinsed 2 × 5 min in acid alcohol (0.1 N HCl in 70% ethanol). Slides were dehydrated in graded ethanol solutions and allowed to air dry in the dark. Once dry, PAFS stained slides were coverslipped with Canada balsam mounting medium (50% Canada balsam resin, 50% methyl salicylate; Fisher Chemicals).

Immunohistochemistry:

Identification of Clara, ciliated, and proliferating cells was performed by triple-immunohistochemical labeling. De-waxed tissue sections were placed first in absolute

ethanol 2 × 10 min, followed by 3% H_2O_2 in methanol for 15 min to quench endogenous peroxidase activity, and then fully re-hydrated. Following antigen retrieval in 100° C sodium citrate solution (10 mM, pH 6.0) 2 × 10 min, non-specific binding sites were blocked with a mixture of 5% normal goat serum and 5% normal horse serum in PBS. Clara cells were labeled using a polyclonal rabbit-anti-mouse-CCSP antibody (1:20,000, 1 h, 25° C; ref. 24) followed by incubation with a directly conjugated horseradish peroxidase (HRP)-labeled goat-anti-mouse-IgG secondary antibody (1:100, 30 min, 25° C, Jackson Immunchemicals). 3–3' diaminobenzidene (DAB) was used as the substrate chromagen for CCSP labeling, and normal rabbit serum was used as a negative control. Ciliated cells were labeled using a monoclonal mouse-anti-acetylated tubulin antibody (1:100,000, 4° C, overnight, Sigma; ref. 25) followed by incubation with a biotinylated horse-anti-mouse (rat adsorbed) secondary antibody (1:100, 30 min, 25° C, Vector Labs, Burlingame, VT), then followed by streptavidin-HRP labeling using Vector VIP as the substrate chromagen. Proliferating cells were labeled by detecting the nuclear proliferation marker Ki-67 with a monoclonal-rat-anti-mouse-Ki-67 antibody (1:100, 4°, overnight, Dako, Carpinteria, CA) followed by incubation with a biotinylated rabbit-anti-rat (mouse adsorbed) secondary antibody (1:100, 30 min, RT, Vector Labs) and streptavidin-HRP labeling using Vector SG as the substrate chromagen. All antibodies were diluted in PBS with 0.1% Tween 20. There were no detectable interspecies cross-reactivities observed among the secondary antibodies in any of these experiments, and tissue sections were washed in 3% H_2O_2 in ddH_2O (15 min) between labeling steps to fully quench peroxidase activity. As a result of immunolabeling, CCSP was labeled brown, cilia were labeled violet, and proliferating cell nuclei were labeled dark blue/black. Nuclei were counterstained using methyl green. Streptavidin HRP labeling of biotinylated secondary antibodies was performed using the ABC Elite kit (Vector Labs). DAB, SG, VIP, and methyl green were purchased from Vector Labs.

For Rab3 immunofluorescent labeling, serial paraffin sections were de-waxed, rehydrated, and antigen-retrieved as described above. Dual immunofluorescence analysis of CCSP and Rab3 isoforms was carried out on three adjacent serial sections using polyclonal goat anti-CCSP antiserum as described previously (1:8,000; ref. 15) in combination with either mouse-anti-rat-Rab3A (BD Biosciences Pharmingen, San Jose, CA), rabbit-anti-mouse-Rab3B (1:8,000) or rabbit-anti-mouse-Rab3D (1:8,000). For Rabs 3B & 3D, rabbit antisera were raised against the recombinant GST-human Rab3B (residues 168–219) and GST-mouse Rab3D (full length) proteins. The respective open reading frames were subcloned into pGEX-2T vector (Amersham Biosciences), expressed, and purified as fusion proteins according to manufacturer's instructions. Rabbits were injected and boosted twice with 100 μg of purified fusion protein according to a standard protocol (26). To increase specificity, sera were passed consecutively through two Glutathione-Sepharose-GST-Rab3 columns: first ratRab3A column and then humRab3B or musRab3D column for anti-musRab3D and anti-humRab3B serum respectively. Sections were blocked with 5% bovine serum albumin in phosphate buffered saline for 30 min and incubated with primary antibodies diluted in blocking buffer overnight at 4° C. Antigen-antibody complexes were detected simultaneously with Alexa 488-conjugated donkey anti-goat Ig and Alexa 594-conjugated donkey anti-rabbit or anit-mouse Ig (1:500 in blocking buffer; Molecular Probes, Eugene, OR).

Brightfield microscopy:

To enumerate the specific numbers and types of cells described above, tissues were examined by a blinded investigator under brightfield conditions and photographed using a cooled CCD camera (Optronics, Goleta, CA) attached to an Olympus BX-60 compound microscope. Epithelial cell numbers in the intrapulmonary axial bronchus were counted manually in 20 high power fields (100x oil immersion objective) through varying focal planes to ensure accurate quantitation of all cells per field. Counts began at the region most proximal to (but not including) the cartilaginous lobar bronchi in each tissue section, and when possible axial bronchi from multiple lobes were analyzed. After counting the numbers of CCSP, acetylated tubulin, and Ki-67 positive cells in a given field, the images were photographed and the length of basement membrane in the field was measured using ImagePro Plus analysis software (Media Cybernetics, Carlsbad, CA). Data are represented as total numbers of cells/mm basement membrane. At each time point, there were a few cells (~0.5–3% of total) that were neither CCSP nor acetylated tubulin positive (table 1).

Fluorescence microscopy:

For the quantitation of mucin, PAFS stained slides were examined under the 40x objective. Ten fields from the axial bronchi were photographed, and camera settings were managed using MagnaFire 2.1 (Optronics). PAFS staining allows for the accurate quantitation of intracellular mucin content through covalent attachment of sulfited acriflavine to mucin glycoconjugates by the same chemistry utilized in traditional PAS staining, but it allows for increased specificity in image analysis compared to traditional AB-PAS staining. When excited at 380–580 nm and observed at 600–650 nm emission, mucin granules fluoresce red. In addition, due to non-covalent linkage of acriflavine to intracellular nucleic acids, nuclei and cytoplasm (but not mucin granules) fluoresce green when excited at 380–500 nm and observed at 450–475 nm. Upon simultaneous excitation and emission at these wavelengths, the presence of both nucleic acids (e.g., RNA) and carbohydrate-rich macromolecules (e.g., glycogen) in the same cellular compartment (e.g., cytosol and mitochondria) results in diminished red fluorescence detection by the camera due to the overlapping green fluorescence in these structures that results in a yellow emission. Since mucin granules do not contain nucleic acids, they do not fluoresce in the green spectrum and their red fluorescence is not quenched (figure E1). By comparison, the traditional PAS staining method results in high background staining due to the presence of variable levels of intracellular non-mucous PAS positive material that is especially apparent in mucous cells that are not completely filled with mucin. In our experiments, PAFS imaging was performed by exciting specimens using a dual excitation filter (500 nm & 573 nm peaks) and observing specimens using a dual emission filter with peaks at 531 nm (green) and 628 nm (red). For each field an image was first generated using only the red acquisition channel on the camera (590 ms exposure). The same image was then re-photographed using both the red and green channels on the camera (590 ms red, 450 ms green).

For morphometric analysis, the volume density and fluorescence intensity of mucin staining were then measured using ImagePro Plus. First, using images acquired in the red channel alone, the total area and fluorescence intensity of intracellular staining above the basement membrane were measured. Second, using the images photographed under both red and

green fluorescence, the total surface area of the epithelium and the length of the basement membrane in each field were measured. Volume density of mucin staining in the airway epithelium was calculated stereologically as described previously (27;28). Briefly, the ratio of surface area of staining to total surface area of the epithelium was divided by a boundary length measurement, which is a product of the total epithelial surface area, the basement membrane length, and the geometric constant $4/\pi$. As a result, data are presented as the volume of intracellular mucin contents per surface area of the basement membrane. Total fluorescence intensity was measured as the sum total of intensity values within each image divided by the length of basement membrane. In preliminary experiments, red images were acquired over a range of increasing exposure times to determine a linear range of exposure and pixel value thresholds for accurate and repeatable measurement of mucin content. Once determined, settings remained constant for all tissue samples throughout the data acquisition process. Images were acquired by blinded investigators prior to any measurements, after which the images were then analyzed by blinded investigators.

To determine whether CCSP and mucin localizes to the same secretory granules in antigen challenged mice, CCSP immunohistochemistry was performed as stated above in PAFS stained tissues, except that an Alexa-647 conjugated goat-anti-mouse-IgG secondary antibody (1:200, 30 min, 25° C, Molecular Probes, Eugene Oregon) was used. Tissues were observed on an inverted microscope by focusing on 45 consecutive 0.2 μm focal planes followed by constrained-iterative deconvolution (DeltaVision, Applied Precision, LLC, Issaquah, Washington). PAFS mucin staining was photographed as described above. CCSP immunoreactivity, observed using a Cy-5 filter (640 nm Ex./ 680 nm Em.), was photographed and pseudocolored blue. Regions of colocalized red and blue fluorescence overlap were pseudocolored pink.

For immunofluorescent imaging of Rab3 isoforms in the lungs, green and red images were collected sequentially with a computer regulated Spot Camera (Diagnostic Instruments, Sterling Heights, MI) and assembled in Adobe Photoshop (San Jose, California). Overlapping red and green fluorescence appeared yellow. Primary antibodies were omitted either singly or in combination to control for specificity of the secondary antibodies and crossover of the green and red emission signals.

Western blot analysis:

The total amount of CCSP in the lungs was measured by Western blotting. Total protein concentrations from whole lung lysates were measured by bicinchoninic acid assay (Pierce, Rockford, IL). Lysates were then aliquoted and stored at −20° C. Samples (10 μg/lane) were separated by Tris-Tricine SDS-PAGE (15% polyacrylamide) and blotted onto PVDF membranes (0.2 μm pore size). In independent experiments, different aliquots of the same samples were electrophoresed by SDS-PAGE as above, and the gels were stained with Coomassie blue to confirm that the amount and quality of protein samples were similar. Detector Blot Solution (DBS; Kirkegaard & Perry Laboratories, Inc., Gaithersburg, MD) was used to block membranes, and CCSP was probed using rabbit anti-CCSP (1:10,000 dilution) and HRP-labeled goat-anti-rabbit IgG (1:20,000) diluted in DBS followed by chemiluminescent detection (Supersignal West Pico, Pierce).

Electron microscopy:

Lungs from animals used for electron microscopy measurements were perfused with 0.9% saline as above and fixed using modified Karnovsky's fixative as described previously (15). Briefly, lungs were fixed at 10–15 cm pressure via the tracheal cannula for 30 min at room temperature, removed, and immersed in fixative overnight at 4°C. After fixation, the left lung was removed and dissected manually to reveal the axial bronchus in 3–5 mm thick cross-sections. The bronchus was cut into cubes of ~1–8 mm^3, post-fixed in osmium, dehydrated, and embedded in araldite epoxy resin (Ladd Research, Williston, VT). Ultrathin sections (80 nm) were stained in three steps by incubating with lead citrate followed by uranyl acetate and then again with lead citrate. Analysis of the ultrastructure of the non-ciliated cells in the airways was performed using a JEM 200CX electron microscope (JEOL USA, Peabody, MA).

Stimulated secretion of mucin:

Dose response curves to ATP were generated by exposing antigen challenged mice to a 5 min ATP aerosol (0.1–100 mM) three days after antigen exposure. Some mice (n=2) received aerosolized NaCl solution (900 mOsm) to ensure that the effect of aerosolized ATP was selective and not related to hyperosmolarity of the ATP aerosol at any of the dosages used. Ten minutes after aerosolization, mice were euthanized, the lungs were processed for light microscopy and stained with PAFS (see above) for quantitation of intracellular mucin. Mucin secretion in ATP treated mice was measured as decreased PAFS staining (volume density and fluorescence, see above) compared to antigen challenged mice not treated with ATP.

Muc5ac, Rab3D, and CCSP promoter cloning and analysis:

The 5' end of the mouse Muc5ac gene was analyzed by sequence alignment of a mouse bacterial artificial chromosome (BAC) containing the entire Muc5b gene and a previously described 3' portion of Muc5ac (29). Gapped alignment of the BAC with the 5' amino terminal cDNA sequence for human MUC5AC showed 73% sequence identity at a site ~40 kb 5' to the start of the Muc5b gene. This sequence of 4 putative exons of the 5' end of mouse Muc5ac was confirmed by RT-PCR. Total RNA from a mouse lung harvested 3 days after antigen challenge was reverse transcribed (Superscript, Invitrogen-Life Technologies, Carlsbad, CA) and PCR amplified using primers generated against the putative cDNA [5'-CATTTCCCCATGCTCCACAG (sense) and 5'-GTGGTGGTATTAGACTCCTGG (antisense)]. All PCR was carried out using the high fidelity proofreading polymerase Pfu Turbo® (Stratagene, La Jolla, CA). The 416 bp product matched the putative mouse cDNA sequence and contained a translation start site.

PCR of the BAC was used to generate a 1 kb genomic DNA fragment containing the 5' untranslated region (UTR) of mouse Muc5ac. Primer sequences used were 5'-GATGGGCCACAAGGGAAGCC (sense) and 5'-GCTGTGGAGCATGGGGAAATG (antisense) with the antisense primer positioned directly adjacent to the putative translation start site. This fragment was first cloned into pCRII-TOPO Blunt vector and then subcloned into a firefly luciferase reporter vector (pGL3 Basic, Promega, Madison, WI) using the HindIII and XhoI sites in the PCRII and pGL3 multicloning

sites. A 950 bp fragment of the Rab3D 5'-UTR was generated by PCR and subcloning from a genomic DNA fragment reported previously by our laboratory (30). Primer sequences were 5'-**GGTACC**CGACAGAGGGAAACATTGAGG (sense) and 5'-**CTCGAG**CCGCACAGGGCTGCGACCCTCG (antisense) and include restriction endonuclease sites (bold) for subcloning into KpnI (sense) and XhoI (antisense) sites in pGL3 Basic. The pGL3 reporter construct containing 800 bp of the mouse CCSP promoter was generated as reported previously (31).

To test for the induction of genes encoding secretory products and components of the exocytic machinery, relative activities of the Muc5ac, Rab3D, and CCSP promoters were measured in a mouse transformed Clara cell (mtCC1–2) line. Cells were transfected with firefly luciferase-promoter constructs along with the Renilla luciferase control vector pRL-TK (Promega) to normalize for transfection efficiency. Cells grown on 6-well plates were transfected with 200 mmol of test promoter and 20 mmol (50 ng) pRL-TK using Fugene 6 (Roche, Indianapolis, IN). Empty pCRII vector was added to each transfection mixture to raise the total mass of DNA per well to 1 μg. To determine the effects of cytokine stimulation on promoter activity, cells were serum starved for 6 h, followed by 24 h incubation with media containing 100 ng/ml of either recombinant mouse IL-13 (the kind gift of Dr. D. Donaldson) or recombinant mouse EGF (Peprotech, Rocky Hill, NJ). Data are represented as a ratio of firefly luciferase activity to Renilla luciferase activity, and as fold induction relative to the firefly luciferase activity in unstimulated cells.

Statistics:

Quantitative data are presented as means ± standard errors, and statistical analysis was performed using Statview statistical analysis software (Abacus Concepts, SAS Institute, Cary, NC). Histological data were analyzed using analysis of variance, and a p-value of less than 0.05 was considered significant. Studies of promoter activities were analyzed using a paired Student's t-test, and a p-value of 0.025 was considered significant.

Results

Mucin is produced by resident epithelial cells in antigen challegened airways:

Mucous cells are present only rarely in the conducting airways of unchallenged mice, but approximately 60% of proximal airway cells are AB-PAS positive 3 days after aerosol challenge of sensitized mice (figures 1 & 2, table 1). This histochemical change in the airway epithelium is accompanied by dramatic changes in secretory cell ultrastructure. By TEM, Clara cells of the axial bronchus of unchallenged mice contain apically localized electron dense secretory granules (figure 1c & e) and an abundance of mitochondria and smooth endoplasmic reticulum (sER), but little rough endoplasmic reticulum (rER, figure 1c & e). Three days after antigen challenge, the abundant mucous cells of the axial bronchus are filled with electron lucent apical granules (figure 1d & f), and the sER is replaced by rER. Quantitation of airway epithelial cell numbers in the proximal airways by light microscopy shows that the AB-PAS positive cells are apparent at 6 h (~5-fold increase). The numbers of these cells are further increased one day after antigen challenge (>20-fold), peaks at day 7 (>30-fold), and remain elevated through day 28 (>10-fold; figure 2). The

numbers of AB-PAS positive cells decrease significantly from days 21–90 compared to the peak at day 7 (figure 2). There is a small but statistically significant increase (~20%) in CCSP positive Clara cells on days 3 and 21 (figure 2). However, acetylated tubulin positive ciliated cells undergo no significant changes in numbers throughout the time course in these studies (figure 2). No significant changes in the epithelial proliferation index occur at any time point assayed in these studies. There is, however, a trend towards a decrease in the proliferative index at 6 h and 1 d and towards an increase at 2 d and 3 d post challenge compared to the steady state. This phenomenon was attributable to the rare Ki-67 positive cells found in subsets of animals assayed at these timepoints and was limited to CCSP positive cells. Importantly, the absence of induced proliferation at the 6h and 1d time points corresponds with the period when the airway epithelium shows the greatest increase in the appearance of AB-PAS-positive secretory cells (Figure 2), with the numbers of AB-PAS positive cells increasing to 12% (6 h) and 55% (1 d) of the total surface epithelial cell population compared to <3% in controls. We, therefore, conclude that the induction of mucin in antigen challenged mice occurs in resident airway epithelial cells by a mechanism that does not require cell division. These data are consistent with previous findings using modified nucleoside analog uptake (32;33).

Changes in airway epithelial cell secretory products:

To assess the production of the major apical secretory products following antigen challenge, the total amounts of mucin and CCSP were measured. PAFS staining was used to measure changes in intracellular mucin over time. In non-challenged mice, the volume density of mucin produced in the lungs is 0.7 nl/mm^2 basement membrane (figure 3). In antigen challenged mice, the volume density of mucin is significantly increased on day 3 and remains significantly increased through day 28. Measured fluorescence also increases significantly on day 3 and remains so until day 21. By both measures, there is a peak in values on day 7 (15-fold over baseline by volume density and 10-fold by fluorescence) followed by significant decreases on days 14–90. Likewise, the amount of CCSP measured by immunoblot also increases in the lungs of antigen challenged mice from days 3–14 and returns to baseline on days 21–90 (figure 3). During the period in which the amount of mucin and CCSP are increased, there is also an increase in the thickness of the airway epithelium that peaks on day 7. While this increase is not statistically significant, on days 28 and 90 there is a statistically significant decrease in epithelial thickness compared to day 7 that occurs simultaneously with the decline in the production mucin and CCSP (figure 3). Decreased epithelial thickness compared to baseline is also observed 6 h and 28 days following antigen challenge. The fall at 6 h is associated with a decrease in CCSP positive secretory granule content seen immunohistochemically (data not shown, n=2) indicating that loss of cell volume is associated with Clara cell secretion during early inflammatory response to antigen inhalation. By contrast, the decreased thickness on day 28 is associated with the replacement or mucous cells by AB-PAS negative Clara cells (figures 1 & 2, table 1).

Mucin is produced by Clara cells in mouse airways:

In order to determine the cellular source of mucin in the mouse lungs, airways immunostained for CCSP were counterstained with either alcian blue, PAS, or PAFS. In all

cases, mucin granules are present exclusively in CCSP positive cells, and a large proportion of celllular mucin and CCSP are present within the same apical secretory granules (figure 4). Some perinuclear mucin granules are negative for CCSP, while some apical granules are negative for mucin, which may reflect the age or maturation state of each of these granule subtypes. By TEM, the secretory granules of bronchial Clara cells resemble those of their bronchiolar relatives (15) in naïve mice. In antigen challenged mice, 3 days post challenge, large secretory granules of lower electron density replace the small electron dense granules present in naïve mice (figure 1d & f). These more electron lucent mucous granules, which are heterogeneous in size and electron density and often contain electron dense cores, replace virtually all of the small electron dense granules found in the Clara cells of non-challenged mice, though small granules that are present at the apical surface may contain smaller amounts of mucin relative to CCSP (figure 1c–f). Thus, the transition from a non-mucous to a mucous phenotype not only involves the up-regulation of one or more new secretory products in a resident secretory cell population, but the newly synthesized products (i.e., mucins) are packaged together with the constitutively synthesized product (i.e., CCSP) in the same secretory granules (figure 4) indicating that mucin and CCSP are both secreted by redundant signal transduction pathways.

Mucin is produced only by proximal airway Clara cells.

Mucin production in the lung is limited to the Clara cells of the proximal airways (figure 5). In antigen challenged mice, AB-PAS positive material is seen throughout the axial bronchus (generations 3 & 4, figure 5, *panel A*) and the proximal portions of the minor daughter bronchial branches (generation 5, figure 5, *panel B*), but no AB-PAS positive material is seen in the bronchiolar regions of the lungs or more distal airspaces (generation 6, figure 5, *panel C*). By contrast, CCSP positive Clara cells are found throughout the entire conducting airway network from the bronchial airways to the alveolar ducts (*see IHC panels A-C*). Moreover, the same lack of distal airway mucin synthesis occurs in adenosine deaminase (ADA) deficient mice where mucous overproduction occurs in response to a systemic stimulus that causes severe airway inflammation, mucus hypersecretion, airway obstruction, and distal airway remodeling (figures S1 & E2; ref. 34) and in mice in which IL-13 has been instilled intranasally (data not shown). These results indicate that only the Clara cells in the proximal airways of mice are capable of producing mucin, and that there is a strict spatial restriction of mucin synthesis at a point midway through the fifth airway generation.

Regulated exocytosis of mucin:

To establish whether airway epithelial cells carry the molecular signature of regulated exocytic cells, the expression of Rab3 proteins was tested. In neurons, Rab3A regulates release of synaptic vesicles from axon terminals (20). In polarized epithelial cells, Rab3B regulates transcytosis from the basolateral to the apical surface (35), and Rab3D regulates secretion of stored exocytic granules (36). We found that Rab3A is restricted to the basolateral region of cells in neuroepithelial bodies while Rab3B is expressed in both CCSP positive and CCSP negative (presumably ciliated) epithelial cells throughout the conducting airways and in the lung periphery (figure 6). Rab3D, however, is restricted to the CCSP positive Clara cell population in the conducting airways (figure 6), and punctate staining of cells in the lung periphery is also seen, presumably in alveolar Type II cells (37). Both

Rab3B and Rab3D continue to be expressed in the Clara cells of antigen challenged mice (data not shown). Thus, in the basal state, the airway epithelium is comprised of diverse cell populations that utilize multiple trafficking pathways for secretion. Clara cells specifically express both preformed exocytic CCSP-containing granules and a molecular marker that defines regulated apical secretory pathways.

Mucous cells contain apical granules characteristic of regulated exocytic cells, express components of a conserved regulated exocytic machinery, and respond to purinergic agonists and other ligands by secreting mucins *in vitro* (38;39). To test whether mucous cells are indeed capable of undergoing regulated exocytosis *in vivo*, dose response curves to inhaled ATP were generated in mice 3 days following antigen challenge. Inhaled ATP (100 mM) caused an acute decrease in the amount of stored mucin seen in AB-PAS stained tissues (figure 7a & b). By TEM, mucin granules are frequently observed fusing with the plasma membrane and releasing their contents into the airway lumen (figure 7c), whereas these fusion events are rarely observed in antigen challenged mice not exposed to ATP (see figure 1d). Quantification of secretion in PAFS stained tissues over a dose response range of 0.1–100 mM shows that the total amount of mucin remaining in the airway epithelium following 100 mM ATP is ~3 nl/mm^2 (5.0 AU/mm) as compared to >6 nl/mm^2 (9.8 AU/mm) in antigen challenged mice that did not receive ATP (figure 7d–f). This decrease constitutes a release of 50% of intracellular stores, since the amount of mucin in non-antigen challenged mice is <1 nl/mm^2 (2.2 AU/mm; figure 7). The effect of ATP on mucin secretion appeared to be receptor mediated and not simply due to hypertonicity, since there was no effect on PAFS staining in mice exposed to 900 mOsm saline (5.2 ± 2.4 nl/mm^2, 11.3 ± 3.9 AU; n=2). Thus, Clara cells in antigen challenged mouse airways produce and store mucin and are capable of secreting mucin stores in a dose dependent regulated exocytic fashion in response to purinergic stimulation.

Induction of genes for secretory products and exocytic machinery in Clara cells:

In order to identify mechanisms that regulate the expression of Clara cell secretory products and exocytic machinery in the naïve and allergic states, we measured the relative promoter activities of CCSP, Muc5ac, and Rab3D in mouse transformed Clara cells. Transfection of mtCC1–2 cells with luciferase reporter constructs demonstrates significant constitutive activity of the CCSP and Rab3D promoters but no significant activity of the Muc5ac promoter above that observed in cells transfected with the empty pGL3 vector (figure 8). Stimulation of mtCC1–2 cells with IL-13 or EGF causes 20- and 30-fold increases in Muc5ac promoter activity, respectively. The magnitude of these significant increases in promoter activation corresponds with both the robust antigen-induced mucin synthesis consistent with the histochemical (figures 1–3), immunohisotchemical (figure 4), and Western blot findings (figure 3) *in vivo*. By comparison, the modest inductions in CCSP and Rab3D promoter activities in EGF and IL-13 treated mtCC1–2 cells corresponds with their continued expression in antigen challenged lungs *in vivo* (figure 2–4). These results indicate that the novel induction of mucin expression by allergic stimulation in the lungs of mice represents the activation of a new secretory product gene (Muc5ac) in addition to, rather than in replacement of, the resident secretory product (CCSP) as well as the

continued expression of a genes encoding components of the regulated exocytic machinery, demonstrated in this case by Rab3D.

DISCUSSION

In the current studies, we identify the ontogeny of antigen-induced mucous cells in the intrapulmonary mouse airways as deriving from the resident CCSP-expressing secretory cells of the epithelium. This change in phenotype does not depend upon proliferation (table 1) and is restricted to CCSP-expressing cells of the tracheobronchial airways but not the CCSP-expressing cells of the bronchioles (figure 5). Differentiation of Clara cells into mucous cells results in dramatic histopathological changes seen by the induction of granular AB-PAS and PAFS positive staining (figure 1–3) and by marked ultrastructural reorganization (figure 1). ‘Metaplasia’ is the term that has been used historically to describe this histopathological change in the airway epithelium. However, the molecular and functional characteristics of the Clara cell are retained in mucous cells. These traits include the expression of genes for apically secreted products (CCSP, figures 2–4), of components of the regulated apical secretory apparatus (Rab3D, figures 6 & 8), and of the capacity for regulated exocytosis (figure 7). The relative continuity in cellular phenotype during mucous cell differentiation--where most of the change in appearance of the epithelium during airway inflammation results simply from the up-regulation of one or more mucin genes by resident Clara cells--contrasts with the more global change in phenotype during airway squamous metaplasia, in which a cell type appears with fundamentally different structure and function and with widespread changes in gene expression compared to cells normally present in the airway epithelium.

In the lungs of mice, the airways from the trachea to the terminal bronchioles are lined predominantly by interdigitating ciliated cells and CCSP-producing Clara cells. The mixture of these two cellular populations serves several functions that include establishing a physical barrier to xenobiotics, acutely responding to inhaled toxicants and pathogens, modulating the trafficking and adhesion of inflammatory cells, and clearing all of these from the lung. Very little gel-forming mucin is produced by the airway epithelium in naïve mice as indicated by the lack of AB-PAS or PAFS positive granular staining seen by light microscopy (figures 1–3), and by the lack of electron lucent granules seen by TEM (figure 1). Thus, under normal conditions the airway epithelium maintains homeostasis through secretory and ciliary means without the need for secreting copious amounts of mucin. In the current study, a single inhaled antigen challenge causes a >30-fold increase in the number of mucous cells (figure 2) and a >15-fold increase in the amount of intracellular mucin packaged into their exocytic granules. Mucin synthesis is localized to CCSP positive cells, indicating that the cellular origin of mucous cells is the Clara cell (figure 4) and that the process of mucin production in these cells results from the induction of an additional secretory product (mucin) without any concomitant loss of the major apical secretory product in the basal state (CCSP). In fact, CCSP production increases in antigen challenged mouse airways (figure 3), in agreement with previous work showing that the allergic cytokine IL-13 increases CCSP production in rat airways (40). One mechanism for allergic stimulation of mucin and CCSP production appears to be mediated by the activation and up-regulation of Muc5ac and CCSP promoter function (figure 8). Whether

this transcriptional up-regulation is complemented by the post-transcriptional regulation seen *in vitro* (41) is not yet determined. Because there is such a dramatic increase in the amount of both mucin and CCSP, and possibly other secreted polypeptides such as defensins and cathelicidins (42), coupled with only a slight increase in CCSP-expressing cell number, antigen-induced mucous cell differentiation could thus be described as the up-regulation of the apical secretory function of specialized resident secretory cell population (i.e., the CCSP-expressing Clara cells). Ultrastructurally this is evident, since the amount of rough endoplasmic reticulum, the site of synthesis of secreted proteins, and the number of secretory granules are both increased in mucin-producing Clara cells following antigen challenge (see figure 1).

Once established, the mucous phenotype resolves after 3–4 weeks, though resolution is incomplete, since even 90 days following antigen challenge the number of mucous cells (~25% of total) and the total amount of mucin stored in the airways (~2-fold higher than baseline) do not return to the low levels seen in naïve mice (figures 2 & 3). This prolonged remodeling is even more dramatic in parainfluenza infected mice where the maximal level of mucin production seen acutely persists for a full year (43) through a process that likely invokes the ability of mucous cells to proliferate (32). Resolution of the mucous phenotype in antigen challenged mice appears to be mediated in part by apoptotic pathways (44), but whether mucous cell differentiation is an irreversible event requiring apoptotic resolution or a labile form of specification in which individual Clara cells reversibly terminate mucin synthesis is not yet clear. We did not observe a significant increase in the rate of cell division during the resolution phase of mucous overproduction (table 1). However, even a small increase in the rates of apoptosis and proliferation in the airway epithelium from days 21–28 that were not measurable in our studies--but have been shown by others (33)--could nonetheless suffice to replace most of the mucous cells with non-mucous Clara cells. Experimental manipulation of both apoptotic and proliferative pathways may be necessary to answer this question.

A gross anatomical constraint exists on the ability of Clara cells to produce mucin in the lungs. In antigen challenged mice, virtually all of the Clara cells in the first two generations of intrapulmonary airways synthesize mucin (figure 5). However, secretory (Clara) cells in the distal regions do not respond by producing mucin, despite the presence of mucin-inducing stimuli in this study and in other models of mucous overproduction, such as repeated antigen challenge (32), IL-13 instillation (Evans and Dickey, unpublished observation), and ADA deficiency (figures E2 & E3). The precise molecular mechanisms involved in restricting mucin synthesis to the proximal airway Clara cells are not yet defined, but other Clara cell cell products are also restricted to different anatomical subcompartments in the airways. A recent study identified other members of the secretaglobin (Scgb) family (of which CCSP is the founding member), including Scgb3A1 that, like mucin, is expressed selectively in the proximal airway secretory cells of mice and humans (45). Restriction of secretory products such as mucins to the proximal airways serves at least two functions. First, the hypersecretion and impaction of mucins in the most distal airways could have catastrophic results if small airways become occluded as occurs in fatal human obstructive lung diseases (1–4;46), or if the highly adhesive mucus is inhaled into the alveolar space. Second, entrapment of particles and pathogens by mucus adhesion in the

proximal rather than the distal airways decreases the chances of alveolar exposure that could result in systemic infection or in impaired gas exchange caused physically or by alveolar inflammation. Anatomically restricted distribution of epithelial cell types is a feature common to other organ systems as well. In the intestinal tract, the proportions of goblet cells lining the alimentary lumen vary among segments. In the jejunum, where most nutrient absorption occurs, there are few goblet cells, while in the distal ileal segment of the small intestine and throughout the large intestine, where only salt and water are absorbed, the number and the proportion of goblet cells increase greatly. Thus, there is a constraint on the presence of goblet cells in these functionally different gross anatomical regions (47). Similarly, spatial restriction of epithelial cell types is apparent within the micropatterning of individual intestinal compartments. In the proximal ileum, which contains the greatest mixture of secretory and non-secretory cells, mature epithelial cells are derived from progenitor cell pools located at the bases of the villi adjacent to the crypts. These differentiate into absorptive enterocytes that rise lumenally along the villi and to secretory Paneth, enteroendocrine, and goblet cells that both rise lumenally along the villi and descend into the crypts. Commitment of secretory cell subsets to a specific pathway is regulated by their positions either in the crypts (Paneth cells) or the villi (enteroendocrine cells and goblet cells) despite their derivation from a common progenitor cell pool (48;49). Thus, the determination of epithelial cell secretory function is regulated by anatomical constraints that pattern gene expression and differentiation and thereby locally specify secretory product expression and release to distinct anatomical regions and microdomains. In the mouse conducting airways, secretory cells located at all levels of the proximal-distal axis are defined by expression of the molecular marker CCSP. However, the structure and function of these cells varies with position along this axis and these distinctions are a likely determinant of regionally-specific roles played by the upper and lower airway in lung homeostasis. Analysis of epithelial injury and repair has shown that the tracheobronchialepithelium and the more distal bronchiolar epithelium arise from regionally distinct progenitor cell populations. The mature surface cells of the tracheobronchial epithelium differentiate from basal cell progenitor pools (50;51) while variant CCSP-expressing cells (vCE) sequestered within neuroepithelial bodies or in the bronchioalveolar duct junction (BADJ) serve as epithelial stem cells for the bronchioles (25). The present study suggests that CCSP-expressing cells that arise from basal cell progenitors are uniquely responsive to metaplastic signals elicited by ovalbumin sensitization and challenge (figures 4–5) and that this property distinguishes proximal basal cell derived secretory cells from distal vCE-derived secretory cells. This anatomic limitation of antigen responsiveness may reflect lineage distinctions between proximal and distal secretory cell populations and/or a level of epigenetic control exerted by the microenvironment on the differentiation potential of distinct precursors of the secretory cell.

In the mature lung, spatial restriction of mucous cells to the tracheobronchial airways may result from developmentally regulated patterning cues that affect mucin synthesis. The lungs arise from the embryonic foregut, and the developing airways undergo successive branching steps that generate increasing numbers of airways of decreased diameter (for review, see ref. 52). The transcription factors HFH-4 (Foxj1) and HNF-3β (Foxa2) regulate branching and morphogenesis early in lung development (53;54), but they also regulate the

cell specific gene expression of mature epithelial cell proteins such as the cilia component β-tubulin IV (HFH-4; ref. 55) and CCSP (HNF-3β; ref. 56). Distal airway branching and alveolarization are mediated by Nkx2.1 (TTF-1; ref. 57) and GATA-6 (58), which also regulate differentiation and the production of surfactant proteins in terminal bronchiolar Clara cells and type II pneumocytes (58–60). These differential patterns of transcription factor activation may restrict the expression of mucin genes, biosynthetic enzymes, or components of mucin-inducing Th2 and EGF signal transduction pathways to the proximal airway epithelium and could thus provide a mechanism for controlling gene expression patterns that distinguish secretory cells of the proximal basal cell lineage and the distal vCE lineage.

Having compared the anatomical and morphological characteristics of airway Clara and mucous cells, we tested whether the airway epithelium also possesses the conserved molecular signature and functional features of regulated exocytic cells. Rab proteins comprise a family of small Ras-related GTPases that ubiquitously regulate interorganellar vesicular transport (19;20). Approximately 60 Rab GTPases are found in the mouse and human genomes, and individual Rab proteins are highly specific to particular steps of transport. Thus, Rab proteins serve as excellent markers of subcellular compartments. The Rab3 subfamily is associated with regulated exocytic processes. In *C. elegans*, there is a single Rab3 protein that functions in synaptic vesicle localization to the active zone of exocytosis (61). In contrast, *S. cerevisiae* lacks a regulated secretory pathway and a Rab3 ortholog, and contains only a constitutive secretory pathway regulated by the Rab8 ortholog Sec4p (62). Vertebrates contain four Rab3 proteins: Rab3A and Rab3C are predominantly found in neurons, where they localize to synaptic vesicles and regulate release (20); Rab3D has been localized to the regulated secretory granules of exocrine pancreatic and salivary epithelial cells (36;63), mast cells (64), and several types of endocrine cells (65), and has been implicated in regulation of granule secretion in several of these cell types (65–67); Rab3B has been localized to the region of the adherens junction of colonic epithelium (68), but studies of a possible role in regulated secretion have been confusing and sometimes contradictory (69–71). Recently, we and collaborators found that Rab3B localizes to endosomes in MDCK epithelial cells and functions in regulating the loading of pIgR-IgA complexes into transcytotic vesicles (35). Thus, Rab3B is not a functional isoform of the other Rab3 proteins in the regulation of exocytosis; rather, its function appears to have diverged in the evolution of higher eukaryotes to the regulation of epithelial transcytosis. Our current localization of Rab3 proteins in airway epithelial cells is consistent with the above findings from other tissues. Rab3A is found only in neuroendocrine cells (figure 6) where it is located in the basolateral cytoplasm (see inset), presumably on small dense core vesicles that are seen by electron microscopy in this location (72). These vesicles are well positioned to signal to neighboring epithelial cells and to submucosal afferent neurons by basolateral exocytosis. Rab3B is found in both ciliated and secretory cells (figure 6), where it may function in transcytosis of IgA by both cell types. Rab3D is found only in Clara cells and mucous cells in the airways, where it is located in the apical cytoplasm (figure 6). Based on studies in other regulated secretory cells, Rab3D in the airway presumably localizes on the surface of electron dense apical granules in Clara cells and electron lucent mucin granules in mucous cells and regulates their release in

response to extracellular signals. Confirmation of the subcellular localization and functions of Rab3 proteins in airway epithelial cells by confocal and immunoelectron microscopy and by phenotypic analysis of mice with mutations in Rab3 genes is underway in our laboratories. Unlike Muc5ac, promoter activation and transcription of the Rab3D gene varies little during mucous induction (figure 8), suggesting continuity of the identity of Clara cells as specialized apical regulated secretory cells during this adaptation to inflammatory stimulation.

Regulated secretory processes are rate-limited by the activation of signaling pathways, so secretory products accumulate intracellularly; in contrast, consitutive secretory processes are rate-limited by the synthesis of secreted products (e.g. cytokines and chemokines) that are rapidly transported to the cell surface for extracellular release, so secretory products do not accumulate. Since mucous cells express both secretory granules and a marker that identifies the regulated exocytic pathway, we tested whether mucous cells in antigen challenged mice behave functionally as *bona fide* regulated exocytic cells. Purinergic receptor agonists are powerful mucin secretagogues *in vitro* (38;39). Moreover, in differentiated airway epithelial cell cultures, ATP induces mucin secretion, while UTP induces both mucin secretion and mucin gene expression (38). *In vivo*, exposure of antigen challenged mice to aerosolized ATP results in a rapid dose dependent decrease in stored mucin content (figure 7). It is clear then, that stores of intracellular mucin can be acutely released in response to inhaled stimuli by a regulated exocytic mechanism. Damage to alveolar epithelial cells causes ATP release and paracrine acitvation of purinergic receptors (73). In the bronchial airways, the release of ATP or UTP by damaged epithelial cells could also play an important role in stimulating neighboring secretory cells to eliminate the damaging agent through both acute secretion and long term up-regulation of the secretory phenotype.

Mucus hypersecretion has been long recognized to contribute to the morbidity and mortality of obstructive airway diseases, but effective treatments have largely lagged behind. While mouse airways are lined predominantly by CCSP-expressing Clara cells from the proximal trachea to the terminal bronchioles, in humans, Clara cells are abundant only in bronchioles. In healthy humans, goblet cells found in the bronchiolar airways also express CCSP, indicating that the Clara cell is a source of mucin in the distal lungs of humans (14). In humans who die from fatal asthma, mucus plugging is present in >90% of the cases (74) and is thought to be the key contributor to lethality (2;3;74). In the lungs of smokers, there is an increase in mucous cells and a decrease in morphologically-identifiable Clara cells in the bronchioles as well (75;76). Thus, recognition that goblet cells derive from Clara cells and that goblet cells continue to secrete CCSP has important implications for the genetic modeling of inflammatory airway diseases in mice, and possibly for cell-specific treatment of human airway obstruction. For example, if the CCSP promoter is used to target gene expression to Clara cells in mice, our data indicate that transgene expression can be expected to increase during acute antigen-induced mucous cell metaplasia rather than decrease as might be expected if the fundamental identity between Clara cells and goblet cells and the up-regulated expression of CCSP during mucous differentiation were not recognized. Further studies assessing changes in CCSP and mucin-expressing cells are needed to determine the whether differentiation characteristics of these cell types is similar under chronic inflammatory conditions such as human asthma. The ability to express CCSP

promoter-driven immunomodulatory genes in the airways in the basal state that could be acitvated further during airway inflammation could also be an attractive gene therapy option in humans. In summary, our studies indicate that the Clara cell is a highly responsive airway epithelial cell type capable of rapidly responding to inflammatory stimuli, and they provide a framework for identifying potential cellular and genetic targets that may be used to treat a wide range of inflammatory lung pathologies whose common feature is mucus hypersecretion.

Supplementary Material

Refer to Web version on PubMed Central for supplementary material.

Acknowledgments

This work was funded by NIH grants HL069650 (C.E.), AI046773 (A.B.), HL070575 & ES008964 (B.S.), and HL043161 & HL072984 (B.D.). The authors wish to thank Blaga Iankova and Evelyn Brown for their technical expertise, Dr. Vernon Knight and Dr. Brian Gilbert for assistance with aerosol measurements, Dr. Debra Donaldson (Department of Respiratory Diseases, Wyeth Research, Cambridge, MA) for recombinant IL-13, and Dr. Roberto Adachi and Dr. Rolando Rumbaut for assistance in fluorescence microscopic analyses.

Reference List

1. Hogg JC, MACKLEM PT, and Thurlbeck WM Site and Nature of Airway Obstruction in Chronic Obstructive Lung Disease. New England Journal of Medicine 1968;20;278(25):1355–60. [PubMed: 5650164]
2. Dunnill MS The Pathology of Asthma, With Special Reference to Changes in the Bronchial Mucosa. J.Clin.Pathol. 1960;13:27–33. [PubMed: 13818688]
3. Huber HL and Koessler KK The Pathology of Bronchial Asthma. Arch Intern Med 1922;30:689–760.
4. Bedrossian CW, Greenberg SD, Singer DB, Hansen JJ, and Rosenberg HS The Lung in Cystic Fibrosis. A Quantitative Study Including Prevalence of Pathologic Findings Among Different Age Groups. Hum.Pathol. 1976;7(2):195–204. [PubMed: 1262016]
5. Sethi S, Evans N, Grant BJ, and Murphy TF New Strains of Bacteria and Exacerbations of Chronic Obstructive Pulmonary Disease. New England Journal of Medicine 8-15-2002;347(7):465–71. [PubMed: 12181400]
6. Lam J, Chan R, Lam K, and Costerton JW Production of Mucoid Microcolonies by Pseudomonas Aeruginosa Within Infected Lungs in Cystic Fibrosis. Infection and Immunity 1980;28(2):546–56. [PubMed: 6772562]
7. Vestbo J, Prescott E, and Lange P Association of Chronic Mucus Hypersecretion With FEV1 Decline and Chronic Obstructive Pulmonary Disease Morbidity. Copenhagen City Heart Study Group. Am.J.Respir.Crit Care Med. 1996;153(5):1530–5. [PubMed: 8630597]
8. MACKLEM PT, FRASER RG, and BROWN WG Bronchial Pressure Measurements in Emphysema and Bronchitis. J.Clin.Invest 1965;44:897–905.:897–905. [PubMed: 14322023]
9. Grunig G, Warnock M, Wakil AE, Venkayya R, Brombacher F, Rennick DM, Sheppard D, Mohrs M, Donaldson DD, Locksley RM, and Corry DB Requirement for IL-13 Independently of IL-4 in Experimental Asthma. Science 12-18-1998;282(5397):2261–3. [PubMed: 9856950]
10. Wills-Karp M, Luyimbazi J, Xu X, Schofield B, Neben TY, Karp CL, and Donaldson DD Interleukin-13: Central Mediator of Allergic Asthma. Science 12-18-1998;282(5397):2258–61. [PubMed: 9856949]
11. Takeyama K, Dabbagh K, Lee HM, Agusti C, Lausier JA, Ueki IF, Grattan KM, and Nadel JA Epidermal Growth Factor System Regulates Mucin Production in Airways. Proc.Natl.Acad.Sci.U.S.A 3-16-1999;96(6):3081–6. [PubMed: 10077640]

12. Ito T, Udaka N, Yazawa T, Okudela K, Hayashi H, Sudo T, Guillemot F, Kageyama R, and Kitamura H Basic Helix-Loop-Helix Transcription Factors Regulate the Neuroendocrine Differentiation of Fetal Mouse Pulmonary Epithelium. Development 2000;127(18):3913–21. [PubMed: 10952889]
13. Pack RJ, Al Ugaily LH, Morris G, and Widdicombe JG The Distribution and Structure of Cells in the Tracheal Epithelium of the Mouse. Cell and Tissue Research 1980;208(1):65–84. [PubMed: 6248229]
14. Boers JE, Ambergen AW, and Thunnissen FB Number and Proliferation of Clara Cells in Normal Human Airway Epithelium. Am.J.Respir.Crit Care Med. 1999;159(5 Pt 1):1585–91. [PubMed: 10228131]
15. Stripp BR, Reynolds SD, Boe IM, Lund J, Power JH, Coppens JT, Wong V, Reynolds PR, and Plopper CG Clara Cell Secretory Protein Deficiency Alters Clara Cell Secretory Apparatus and the Protein Composition of Airway Lining Fluid. American Journal of Respiratory Cell and Molecular Biology 2002;27(2):170–8. [PubMed: 12151308]
16. Singh G, Singh J, Katyal SL, Brown WE, Kramps JA, Paradis IL, Dauber JH, Macpherson TA, and Squeglia N Identification, Cellular Localization, Isolation, and Characterization of Human Clara Cell-Specific 10 KD Protein. Journal of Histochemistry and Cytochemistry 1988;36(1):73–80. [PubMed: 3275712]
17. Alimam MZ, Piazza FM, Selby DM, Letwin N, Huang L, and Rose MC Muc-5/5ac Mucin Messenger RNA and Protein Expression Is a Marker of Goblet Cell Metaplasia in Murine Airways. American Journal of Respiratory Cell and Molecular Biology 2000;22(3):253–60. [PubMed: 10696060]
18. Li Y, Martin LD, Spizz G, and Adler KB MARCKS Protein Is a Key Molecule Regulating Mucin Secretion by Human Airway Epithelial Cells in Vitro. Journal Of Biological Chemistry 11-2-2001;276(44):40982–90. [PubMed: 11533058]
19. Tuvim MJ, Adachi R, and Dickey BF Traffic Control: Rab GTPases and the Regulation of Interorganellar Transport. News in Physiological Sciences 2001;16:56–61. [PubMed: 11390949]
20. Zerial M and McBride H Rab Proteins As Membrane Organizers. Nature Reviews Molecular Cell Biology 2001;2(2):107–17. [PubMed: 11252952]
21. Koshkina NV, Knight V, Gilbert BE, Golunski E, Roberts L, and Waldrep JC Improved Respiratory Delivery of the Anticancer Drugs, Camptothecin and Paclitaxel, With 5% CO2-Enriched Air: Pharmacokinetic Studies. Cancer Chemother.Pharmacol. 2001;47(5):451–6. [PubMed: 11391862]
22. Koshkina NV, Agoulnik IY, Melton SL, Densmore CL, and Knight V Biodistribution and Pharmacokinetics of Aerosol and Intravenously Administered DNA-Polyethyleneimine Complexes: Optimization of Pulmonary Delivery and Retention. Mol.Ther. 2003;8(2):249–54. [PubMed: 12907147]
23. Fairchild GA Measurement of Respiratory Volume for Virus Retention Studies in Mice. Appl.Microbiol. 1972;24(5):812–8. [PubMed: 4344961]
24. Ray MK, Wang G, Barrish J, Finegold MJ, and DeMayo FJ Immunohistochemical Localization of Mouse Clara Cell 10-KD Protein Using Antibodies Raised Against the Recombinant Protein. Journal of Histochemistry and Cytochemistry 1996;44(8):919–27. [PubMed: 8756763]
25. Reynolds SD, Hong KU, Giangreco A, Mango GW, Guron C, Morimoto Y, and Stripp BR Conditional Clara Cell Ablation Reveals a Self-Renewing Progenitor Function of Pulmonary Neuroendocrine Cells. Am.J.Physiol Lung Cell Mol.Physiol 2000;278(6):L1256–L1263. [PubMed: 10835332]
26. Harlow E and Lane D, Antibodies: A Laboratory Manual. Cold Spring Harbor, N.Y.: Cold Spring Harbor Laboratory; 1988.
27. Harkema JR, Plopper CG, Hyde DM, and St George JA Regional Differences in Quantities of Histochemically Detectable Mucosubstances in Nasal, Paranasal, and Nasopharyngeal Epithelium of the Bonnet Monkey. Journal of Histochemistry and Cytochemistry 1987;35(3):279–86. [PubMed: 2434556]
28. Weibel ER, Sterological Methods. London: Academic Press Inc. Ltd.; 1979.(1).

29. Chen Y, Zhao YH, and Wu R In Silico Cloning of Mouse Muc5b Gene and Upregulation of Its Expression in Mouse Asthma Model. Am.J Respir.Crit Care Med 9-15-2001;164(6):1059–66. [PubMed: 11587997]
30. Adachi R, Nigam R, Tuvim MJ, DeMayo F, and Dickey BF Genomic Organization, Chromosomal Localization, and Expression of the Murine RAB3D Gene. Biochemical And Biophysical Research Communications 7-14-2000;273(3):877–83. [PubMed: 10891340]
31. Ramsay PL, Luo Z, Magdaleno SM, Whitbourne SK, Cao X, Park MS, Welty SE, Yu-Lee LY, and DeMayo FJ Transcriptional Regulation of CCSP by Interferon-Gamma in Vitro and in Vivo. Am.J.Physiol Lung Cell Mol.Physiol 2003;284(1):L108–L118. [PubMed: 12388333]
32. Reader JR, Tepper JS, Schelegle ES, Aldrich MC, Putney LF, Pfeiffer JW, and Hyde DM Pathogenesis of Mucous Cell Metaplasia in a Murine Asthma Model. American Journal of Pathology 2003;162(6):2069–78. [PubMed: 12759261]
33. Trifilieff A, Ahmed E, and Bertrand C Time Course of Inflammatory and Remodeling Events in a Murine Model of Asthma: Effect of Steroid Treatment. Am.J.Physiol Lung Cell Mol.Physiol 2000;279:L1120–L1128. [PubMed: 11076802]
34. Blackburn MR, Volmer JB, Thrasher JL, Zhong H, Crosby JR, Lee JJ, and Kellems RE Metabolic Consequences of Adenosine Deaminase Deficiency in Mice Are Associated With Defects in Alveogenesis, Pulmonary Inflammation, and Airway Obstruction. Journal of Experimental Medicine 7-17-2000;192(2):159–70. [PubMed: 10899903]
35. van IJzendoorn SC, Tuvim MJ, Weimbs T, Dickey BF, and Mostov KE Direct Interaction Between Rab3b and the Polymeric Immunoglobulin Receptor Controls Ligand-Stimulated Transcytosis in Epithelial Cells. Dev.Cell 2002;2(2):219–28. [PubMed: 11832247]
36. Valentijn JA, Sengupta D, Gumkowski FD, Tang LH, Konieczko EM, and Jamieson JD Rab3D Localizes to Secretory Granules in Rat Pancreatic Acinar Cells. European Journal of Cell Biology 1996;70(1):33–41. [PubMed: 8738417]
37. van Weeren L, de Graaff AM, Jamieson JD, Batenburg JJ, and Valentijn JA Rab3D and Actin Reveal Distinct Lamellar Body Subpopulations in Alveolar Epithelial Type II Cells. American Journal of Respiratory Cell and Molecular Biology 2004;30(3):288–95. [PubMed: 12933357]
38. Chen Y, Zhao YH, and Wu R Differential Regulation of Airway Mucin Gene Expression and Mucin Secretion by Extracellular Nucleotide Triphosphates. Am.J Respir.Cell Mol.Biol. 2001;25(4):409–17. [PubMed: 11694445]
39. Abdullah LH, Davis SW, Burch L, Yamauchi M, Randell SH, Nettesheim P, and Davis CW P2u Purinoceptor Regulation of Mucin Secretion in SPOC1 Cells, a Goblet Cell Line From the Airways. Biochem.J 6-15-1996;316(Pt 3):943–51. [PubMed: 8670174]
40. Kim S, Shim JJ, Burgel PR, Ueki IF, Dao-Pick T, Tam DC, and Nadel JA IL-13-Induced Clara Cell Secretory Protein Expression in Airway Epithelium: Role of EGFR Signaling Pathway. Am.J Physiol Lung Cell Mol.Physiol 2002;283(1):L67–L75. [PubMed: 12060562]
41. Voynow JA, Young LR, Wang Y, Horger T, Rose MC, and Fischer BM Neutrophil Elastase Increases MUC5AC MRNA and Protein Expression in Respiratory Epithelial Cells. Am.J Physiol 1999;276(5 Pt 1):L835–L843. [PubMed: 10330040]
42. Cole AM and Waring AJ The Role of Defensins in Lung Biology and Therapy. Am.J.Respir.Med. 2002;1(4):249–59. [PubMed: 14720045]
43. Walter MJ, Morton JD, Kajiwara N, Agapov E, and Holtzman MJ Viral Induction of a Chronic Asthma Phenotype and Genetic Segregation From the Acute Response. J.Clin.Invest 2002;110(2):165–75. [PubMed: 12122108]
44. Shi ZO, Fischer MJ, De Sanctis GT, Schuyler MR, and Tesfaigzi Y IFN-Gamma, but Not Fas, Mediates Reduction of Allergen-Induced Mucous Cell Metaplasia by Inducing Apoptosis. Journal of Immunology 5-1-2002;168(9):4764–71.
45. Reynolds SD, Reynolds PR, Pryhuber GS, Finder JD, and Stripp BR Secretoglobins SCGB3A1 and SCGB3A2 Define Secretory Cell Subsets in Mouse and Human Airways. Am.J.Respir.Crit Care Med. 12-1-2002;166(11):1498–509. [PubMed: 12406855]
46. Simel DL, Mastin JP, Pratt PC, Wisseman CL, Shelburne JD, Spock A, and Ingram P Scanning Electron Microscopic Study of the Airways in Normal Children and in Patients With Cystic Fibrosis and Other Lung Diseases. Pediatr.Pathol. 1984;2(1):47–64. [PubMed: 6542212]

47. Sweetser DA, Birkenmeier EH, Hoppe PC, McKeel DW, and Gordon JI Mechanisms Underlying Generation of Gradients in Gene Expression Within the Intestine: an Analysis Using Transgenic Mice Containing Fatty Acid Binding Protein-Human Growth Hormone Fusion Genes. Genes and Development 1988;2(10):1318–32. [PubMed: 2462524]

48. Clatworthy JP and Subramanian V Stem Cells and the Regulation of Proliferation, Differentiation and Patterning in the Intestinal Epithelium: Emerging Insights From Gene Expression Patterns, Transgenic and Gene Ablation Studies. Mech.Dev. 2001;101(1–2):3–9. [PubMed: 11231054]

49. Yang Q, Bermingham NA, Finegold MJ, and Zoghbi HY Requirement of Math1 for Secretory Cell Lineage Commitment in the Mouse Intestine. Science 12-7-2001;294(5549):2155–8. [PubMed: 11739954]

50. Hong KU, Reynolds SD, Watkins S, Fuchs E, and Stripp BR In Vivo Differentiation Potential of Tracheal Basal Cells: Evidence for Multipotent and Unipotent Subpopulations. Am.J.Physiol Lung Cell Mol.Physiol 7-18-2003;ePub ahead of print.

51. Hong KU, Reynolds SD, Watkins S, Fuchs E, and Stripp BR Basal Cells Are a Multipotent Progenitor Capable of Renewing the Bronchial Epithelium. American Journal of Pathology 2004;164(2):577–88. [PubMed: 14742263]

52. Warburton D, Schwarz M, Tefft D, Flores-Delgado G, Anderson KD, and Cardoso WV The Molecular Basis of Lung Morphogenesis. Mech.Dev. 3-15-2000;92(1):55–81. [PubMed: 10704888]

53. Ang SL and Rossant J HNF-3 Beta Is Essential for Node and Notochord Formation in Mouse Development. Cell 8-26-1994;78(4):561–74. [PubMed: 8069909]

54. Chen J, Knowles HJ, Hebert JL, and Hackett BP Mutation of the Mouse Hepatocyte Nuclear Factor/Forkhead Homologue 4 Gene Results in an Absence of Cilia and Random Left-Right Asymmetry. J.Clin.Invest 9-15-1998;102(6):1077–82. [PubMed: 9739041]

55. Blatt EN, Yan XH, Wuerffel MK, Hamilos DL, and Brody SL Forkhead Transcription Factor HFH-4 Expression Is Temporally Related to Ciliogenesis. American Journal of Respiratory Cell and Molecular Biology 1999;21(2):168–76. [PubMed: 10423398]

56. Sawaya PL, Stripp BR, Whitsett JA, and Luse DS The Lung-Specific CC10 Gene Is Regulated by Transcription Factors From the AP-1, Octamer, and Hepatocyte Nuclear Factor 3 Families. Molecular & Cellular Biology 1993;13(7):3860–71. [PubMed: 8321193]

57. Minoo P, Su G, Drum H, Bringas P, and Kimura S Defects in Tracheoesophageal and Lung Morphogenesis in Nkx2.1(−/−) Mouse Embryos. Developmental Biology 5-1-1999;209(1):60–71. [PubMed: 10208743]

58. Liu C, Morrisey EE, and Whitsett JA GATA-6 Is Required for Maturation of the Lung in Late Gestation. Am.J.Physiol Lung Cell Mol.Physiol 2002;283(2):L468–L475. [PubMed: 12114210]

59. Liu C, Glasser SW, Wan H, and Whitsett JA GATA-6 and Thyroid Transcription Factor-1 Directly Interact and Regulate Surfactant Protein-C Gene Expression. Journal Of Biological Chemistry 2-8-2002;277(6):4519–25. [PubMed: 11733512]

60. Yang H, Lu MM, Zhang L, Whitsett JA, and Morrisey EE GATA6 Regulates Differentiation of Distal Lung Epithelium. Development 2002;129(9):2233–46. [PubMed: 11959831]

61. Nonet ML, Staunton JE, Kilgard MP, Fergestad T, Hartwieg E, Horvitz HR, Jorgensen EM, and Meyer BJ Caenorhabditis Elegans Rab-3 Mutant Synapses Exhibit Impaired Function and Are Partially Depleted of Vesicles. Journal of Neuroscience 1997;17(21):8061–73. [PubMed: 9334382]

62. Salminen A and Novick PJ A Ras-Like Protein Is Required for a Post-Golgi Event in Yeast Secretion. Cell 1987;49:527–38. [PubMed: 3552249]

63. Ohnishi H, Ernst SA, Wys N, McNiven M, and Williams JA Rab3D Localizes to Zymogen Granules in Rat Pancreatic Acini and Other Exocrine Glands. American Journal of Physiology: Gastrointestinal and Liver Physiology 1996;271(3):G531–G538.

64. Tuvim MJ, Adachi R, Chocano JF, Moore RH, Lampert RM, Zera E, Romero E, Knoll BJ, and Dickey BF Rab3D, a Small GTPase, Is Localized on Mast Cell Secretory Granules and Translocates to the Plasma Membrane Upon Exocytosis. American Journal of Respiratory Cell and Molecular Biology 1-1-1999;20(1):79–89. [PubMed: 9870920]

65. Baldini G, Wang G, Weber M, Zweyer M, Bareggi R, Witkin JW, and Martelli AM Expression of Rab3D N135I Inhibits Regulated Secretion of ACTH in AtT- 20 Cells. Journal Of Cell Biology 1-26-1998;140(2):305–13. [PubMed: 9442106]

66. Roa M, Paumet F, Le Mao J, David B, and Blank U Involvement of the Ras-Like GTPase Rab3d in RBL-2H3 Mast Cell Exocytosis Following Stimulation Via High Affinity IgE Receptors. Journal of Immunology 1997;159(6):2815–23.

67. Ohnishi H, Samuelson LC, Yule DI, Ernst SA, and Williams JA Overexpression of Rab3D Enhances Regulated Amylase Secretion From Pancreatic Acini of Transgenic Mice. Journal of Clinical Investigation 1997;100(12):3044–52. [PubMed: 9399951]

68. Weber E, Berta G, Tousson A, St-John P, Green MW, Gopalokrishnan U, Jilling T, Sorscher EJ, Elton TS, Abrahamson DR, and Kirk KL Expression and Polarized Targeting of a Rab3 Isoform in Epithelial Cells. Journal Of Cell Biology 1994;125(3):583–94. [PubMed: 8175882]

69. Lledo P-M, Vernier P, Vincent J-D, Mason WT, and Zorec R Inhibition of Rab3B Expression Attenuates Ca^{2+}-Dependent Exocytosis in Rat Anterior Pituitary Cells. Nature 1993;364:540–4. [PubMed: 8393147]

70. Weber E, Jilling T, and Kirk KL Distinct Functional Properties of Rab3A and Rab3B in PC12 Neuroendocrine Cells. Journal Of Biological Chemistry 1996;271(12):6963–71. [PubMed: 8636125]

71. Iezzi M, Escher G, Meda P, Charollais A, Baldini G, Darchen F, Wollheim CB, and Regazzi R Subcellular Distribution and Function of Rab3A, B, C, and D Isoforms in Insulin-Secreting Cells. Mol.Endocrinol. 1999;13(2):202–12. [PubMed: 9973251]

72. Cutz E, Chan W, Wong V, and Gillan JE Development of Neuroendocrine Cells in Human-Lung - Histochemical, Immunohistochemical, and Ultrastructural-Study. Laboratory Investigation 1982;46(1):3–4.

73. Isakson BE, Evans WH, and Boitano S Intercellular Ca2+ Signaling in Alveolar Epithelial Cells Through Gap Junctions and by Extracellular ATP. Am.J.Physiol Lung Cell Mol.Physiol 2001;280(2):L221–L228. [PubMed: 11159000]

74. Kuyper LM, Pare PD, Hogg JC, Lambert RK, Ionescu D, Woods R, and Bai TR Characterization of Airway Plugging in Fatal Asthma. Am.J.Med. 2003;115(1):6–11. [PubMed: 12867228]

75. Ebert RV and Terracio MJ The Bronchiolar Epithelium in Cigarette Smokers. Observations With the Scanning Electron Microscope. Am.Rev.Respir.Dis. 1975;111(1):4–11. [PubMed: 1111397]

76. Lumsden AB, McLean A, and Lamb D Goblet and Clara Cells of Human Distal Airways: Evidence for Smoking Induced Changes in Their Numbers. Thorax () 1984;39(11):844–9. [PubMed: 6505991]

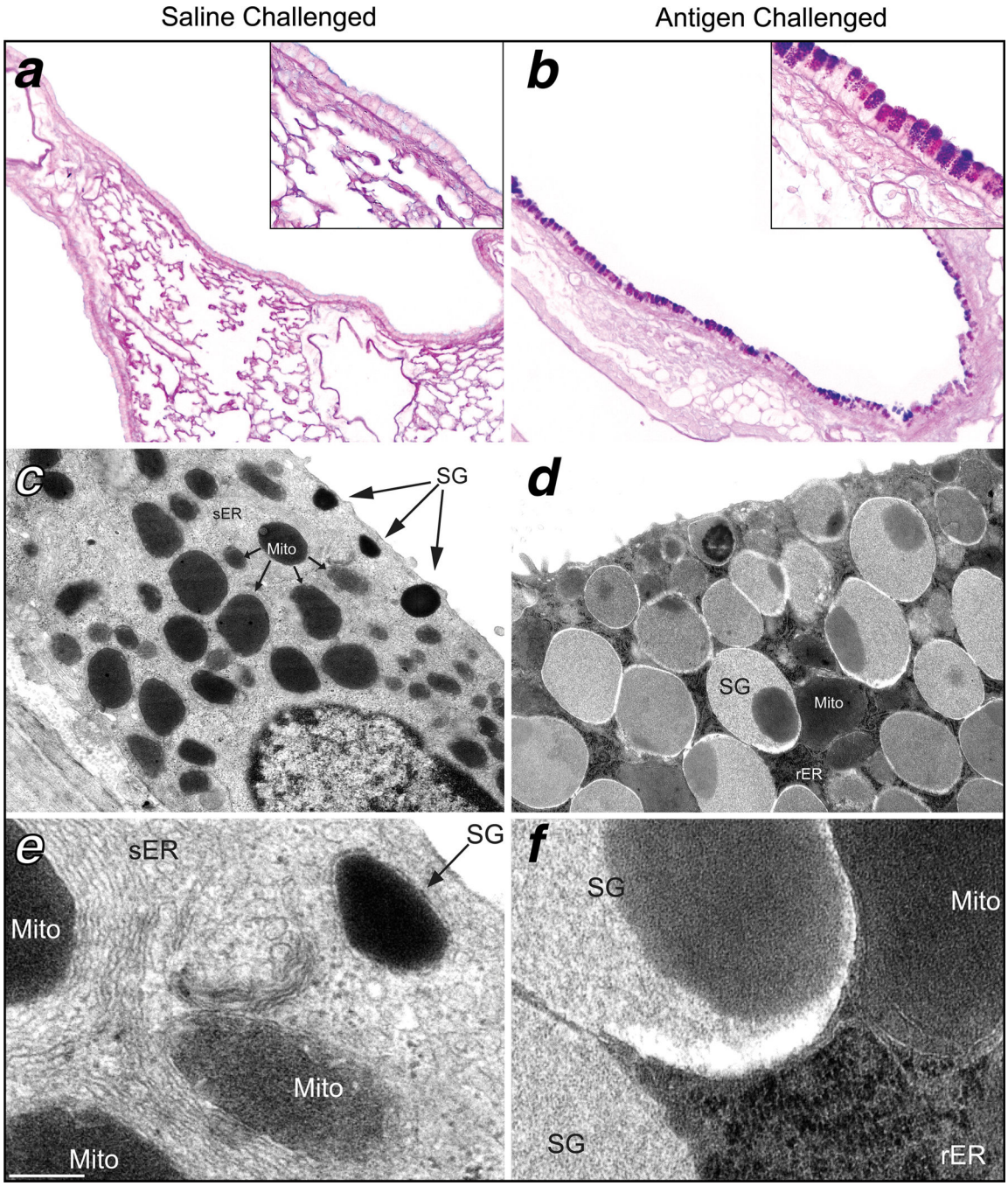

Figure 1.

Antigen challenge causes marked structural changes in mouse airway epithelium. ***Left.*** The airway epithelium of saline challenged mice contains little or no AB-PAS positive mucin granules in the surface airway epithelium seen by light microscopy (*a*). By TEM there is an abundance of smooth endoplasmic reticulum (sER), mitochondria (Mito), and small electron dense apical secretory granules (SG) in the majority of non-ciliated surface epithelial cells in unchallenged animals (*c & e*). ***Right.*** Three days after antigen exposure, the airways demonstrate a marked increase in dark AB-PAS cytoplasmic staining (*b*) specifically within

apical secretory granules (*b inset*). There is also a change in the ultrastructure of bronchial airway secretory epithelial cells indicative of the mucous phenotype (*d*). The cytoplasm of mucous cells contain more SG's that are more electron lucent and often also contain electron dense cores (*d*). There is also a greater abundance of rough endoplasmic reticulum (rER) and decrease in sER in mucous cells (*f*). In brightfield images, the scale bar is 120 μm at low magnification and 25 μm at high magnification. Photomicrographs are representative of 5–6 animals per group. In TEM images, scale bar is 1 μm at low magnification and 150 nm at high magnification. Electron micrographs are representative of 4 mice per group.

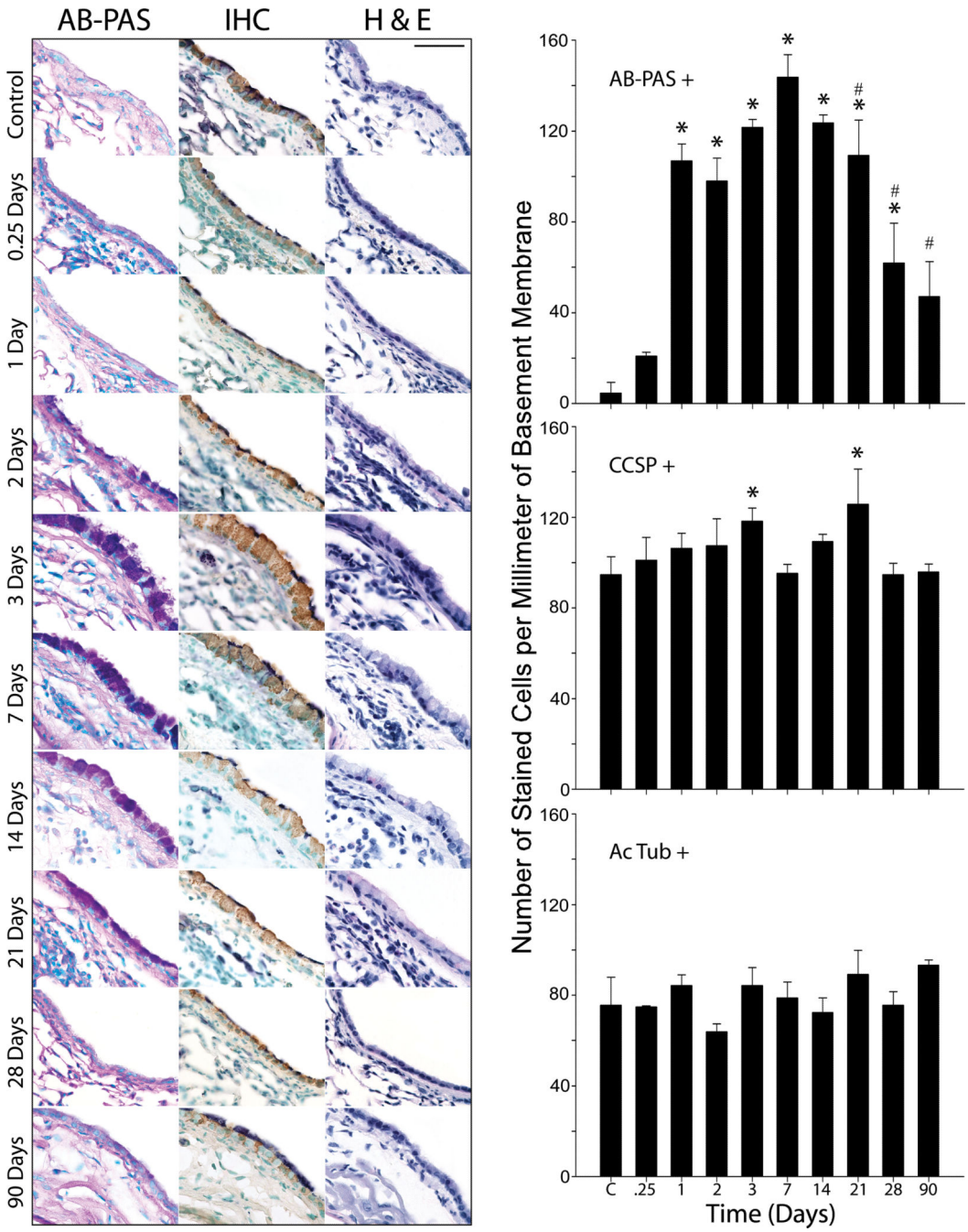

Figure 2.

Antigen challenge causes a transient increase in mucin content in the airways with little alteration in the distribution of Clara and ciliated cells. In antigen challenged mice, the number of AB-PAS positive cells increases significantly 1 day after antigen challenge, peaks at day 7 and partially resolves at days 21–28 (*top graph*). Immunohistochemical staining (IHC column) of CCSP positive Clara cells (CCSP positive) reveals small but significant increases at day 3 and day 21 (*middle graph*). There are no significant changes in the numbers of ciliated cells (acetylated tubulin positive) throughout the timecourse (*IHC column & lower graph*). Hematoxylin & eosin (H & E) staining shows submucosal

inflammation occurring during the period of increase mucin production (days 1–21). Three to six animals were used for each time point except for 0.25 days (n=2). * indicates statistically significant difference from control, and # signifies statistically significant difference from day 7. Scale bar is 50 μm.

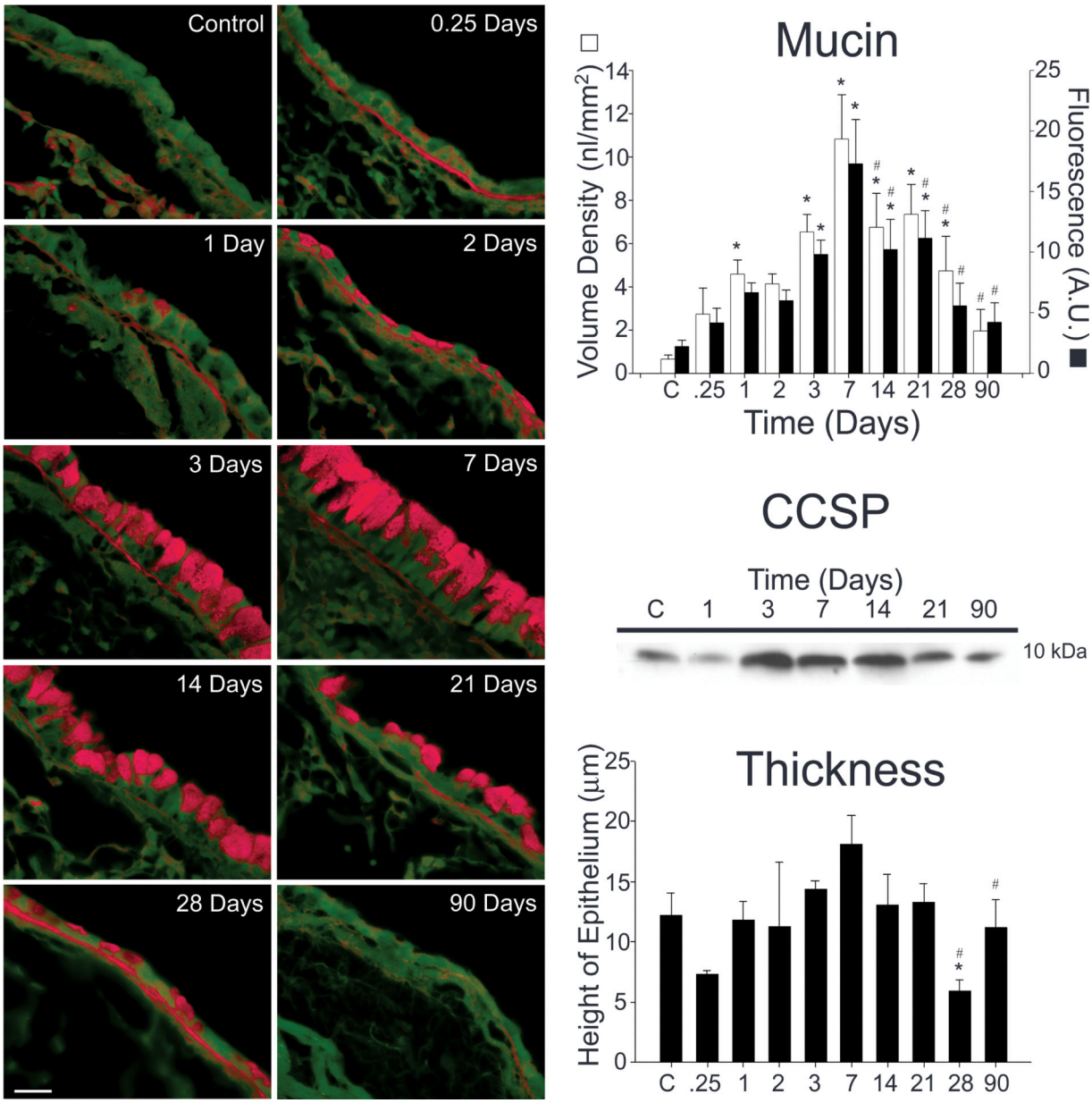

Figure 3.

Mucin and CCSP content both increase during allergic airway inflammation. Tissue sections from antigen challenged mice were stained using a periodic acid fluorescent Schiff (PAFS) method (*left panels*). Mucin content increases as early as 6 h (0.25 days) following antigen challenge, is significantly increased 1 day following antigen challenge, and is maximal at 1 week (*right, upper panel*). Mucin content decreases significantly from peak levels 14–28 days following antigen exposure (*right, upper panel*). CCSP content of the lung was measured by Western blotting. CCSP is produced constitutively in the lungs of control mice (*right, middle panel*). The amount of CCSP increases at days 3–14 and returns to baseline at day 21. There was also an increase in the thickness of the airway epithelium that peaked at day 7 (*right, lower panel*). While this increase was not statistically significant, the decrease

in thickness (seen coincidentally with decreasing mucin and CCSP levels) was significantly lower than unchallenged mice (day 28) and day 7 mice (days 28 & 90). Three to six animals were used for each time point except for 0.25 days (n=2). * indicates statistically significant difference from control, and # signifies statistically significant difference from day 7.

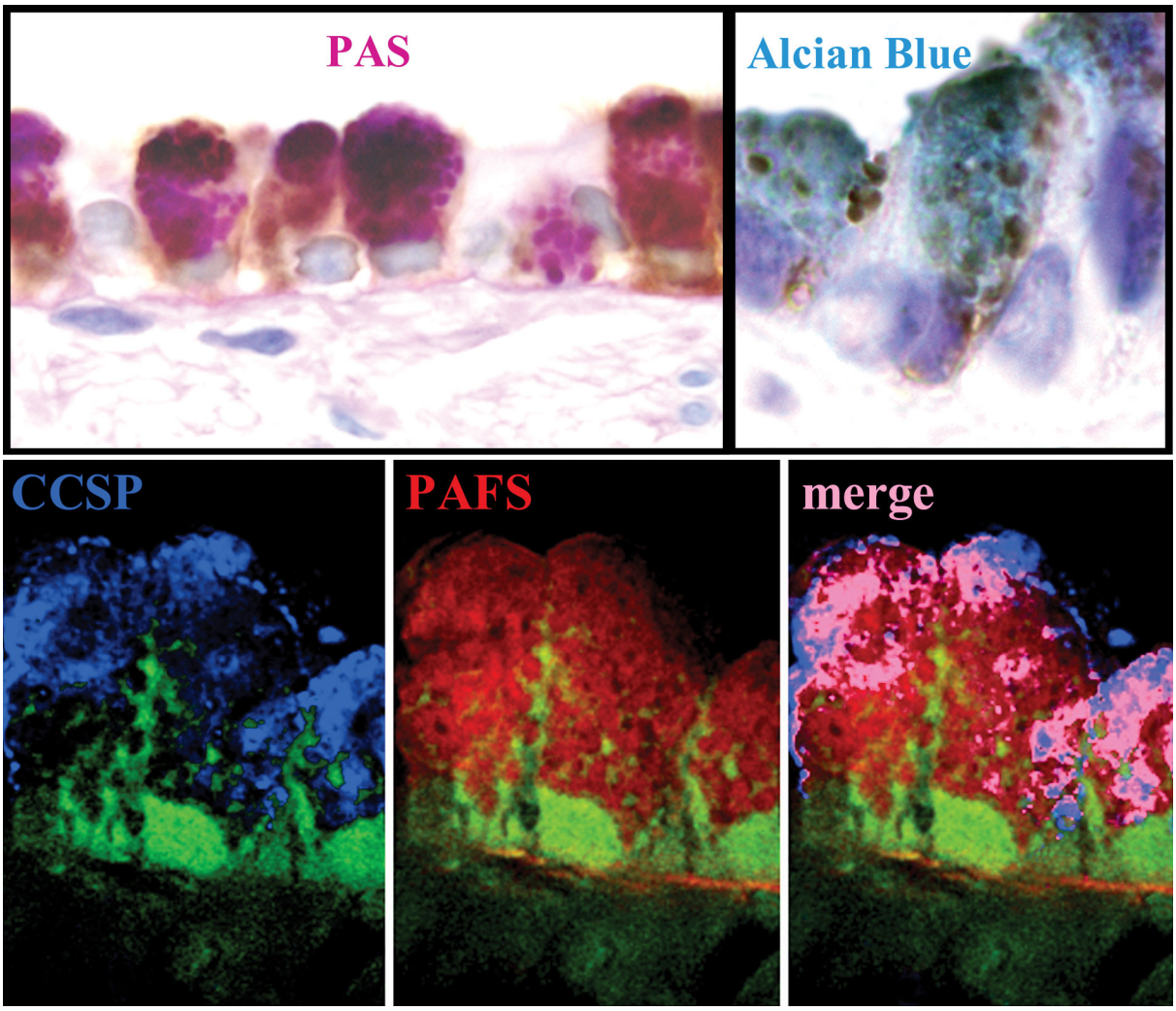

Figure 4.

Mucin is produced by Clara cells in antigen challenged mice. ***Top.*** Airways from antigen challenged mice were stained immunohistochemically for CCSP and counterstained with either PAS (*right*) or alcian blue to stain acidic and sulfated mucins (*left*) to stain neutral mucins. In antigen challenged mice, alcian blue or PAS mucin granule staining colocalizes exclusively to cells immunoabeled positively for CCSP. ***Bottom.*** CCSP and mucin are packaged in the same secretory granules. Colocalization of mucin (red PAFS staining) and CCSP (blue CCSP immunolabeling) was determined by deconvolution microscopy in 0.2 μm optical planes. Pink in the merged image demonstrates colocalization of CCSP and PAFS within apical secretory granules. Scale bar is 10 μm in PAS stained images and 6 μm in alcian blue and PAFS stained images.

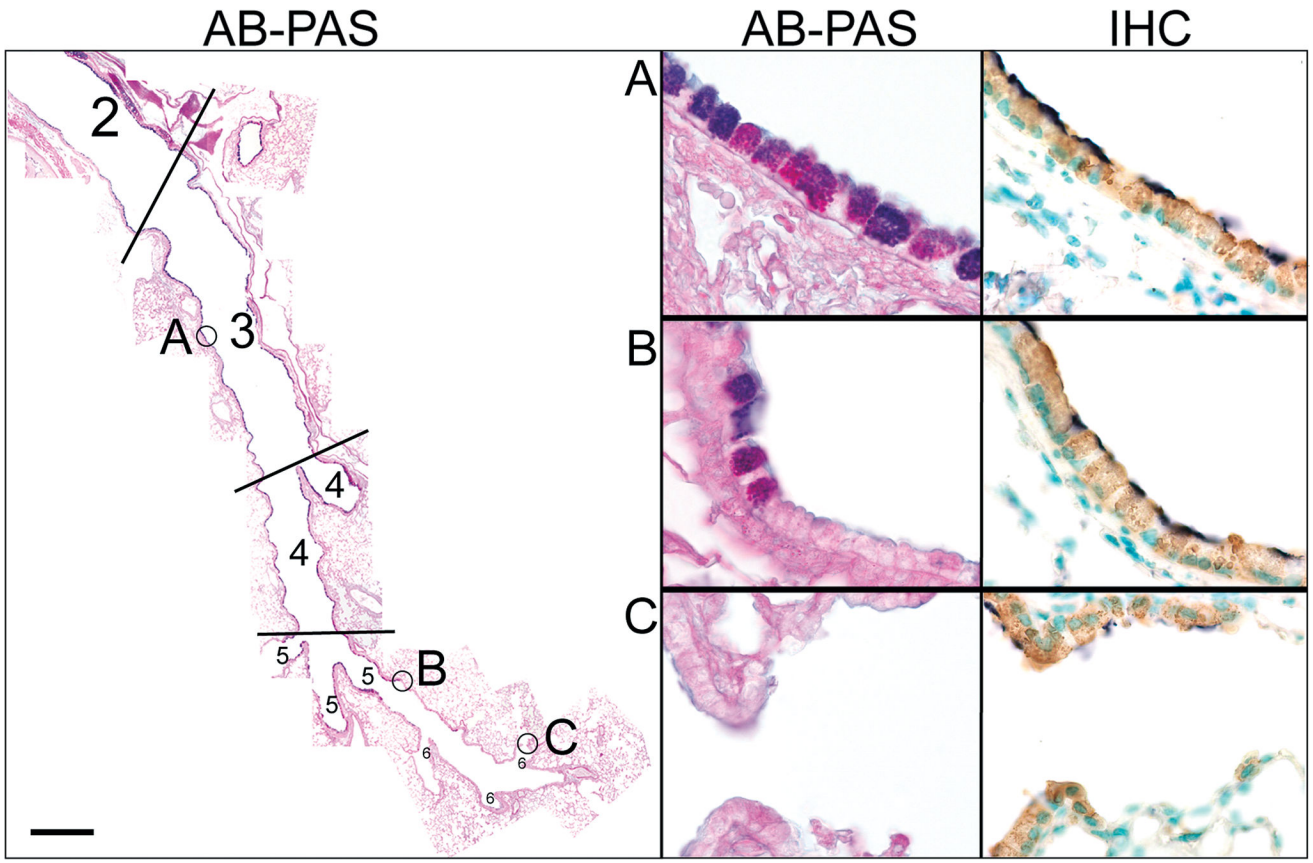

Figure 5.

Mucin production is restricted to proximal airway Clara cells. ***Left.*** Numbers represent specific airway generation starting from the trachea: 1= trachea (not shown), 2=mainstem bronchus, 3=proximal intrapulmonary axial bronchus, 4=distal intrapulmonary axial bronchus, 5=minor daughter bronchiole, 6=terminal bronchiole, 7=alveolar duct (not labeled). Cells containing AB-PAS positive mucin granules can be seen throughout the first four airway generations in antigen challenged mice. The proximal portion of the fifth airway generation contains many mucous cells, but only an occasional mucous cell is present in the distal portion of this airway generation. From the sixth airway generation to the alveolar ducts no mucin producing cells are present. ***Right.*** High magnification of AB-PAS stained airways marked in left panel and immunohistochemical labeling of Clara cells (IHC) in adjacent consecutive sections. *A.* AB-PAS and CCSP positive cells are found ubiquitously in the proximal intrapulmonary airways of antigen challenged mice (generations 3 & 4). *B.* Airway generation five marks a transitional zone that is lined by Clara cells (*right panel*), but AB-PAS positive mucous cells are only present in the proximal region (*left panel*). *C.* No mucous cells are present in terminal bronchiole and alveolar duct Clara cells. Scale bar is 50 μm in low magnification composite image and 5 μm in high magnification images.

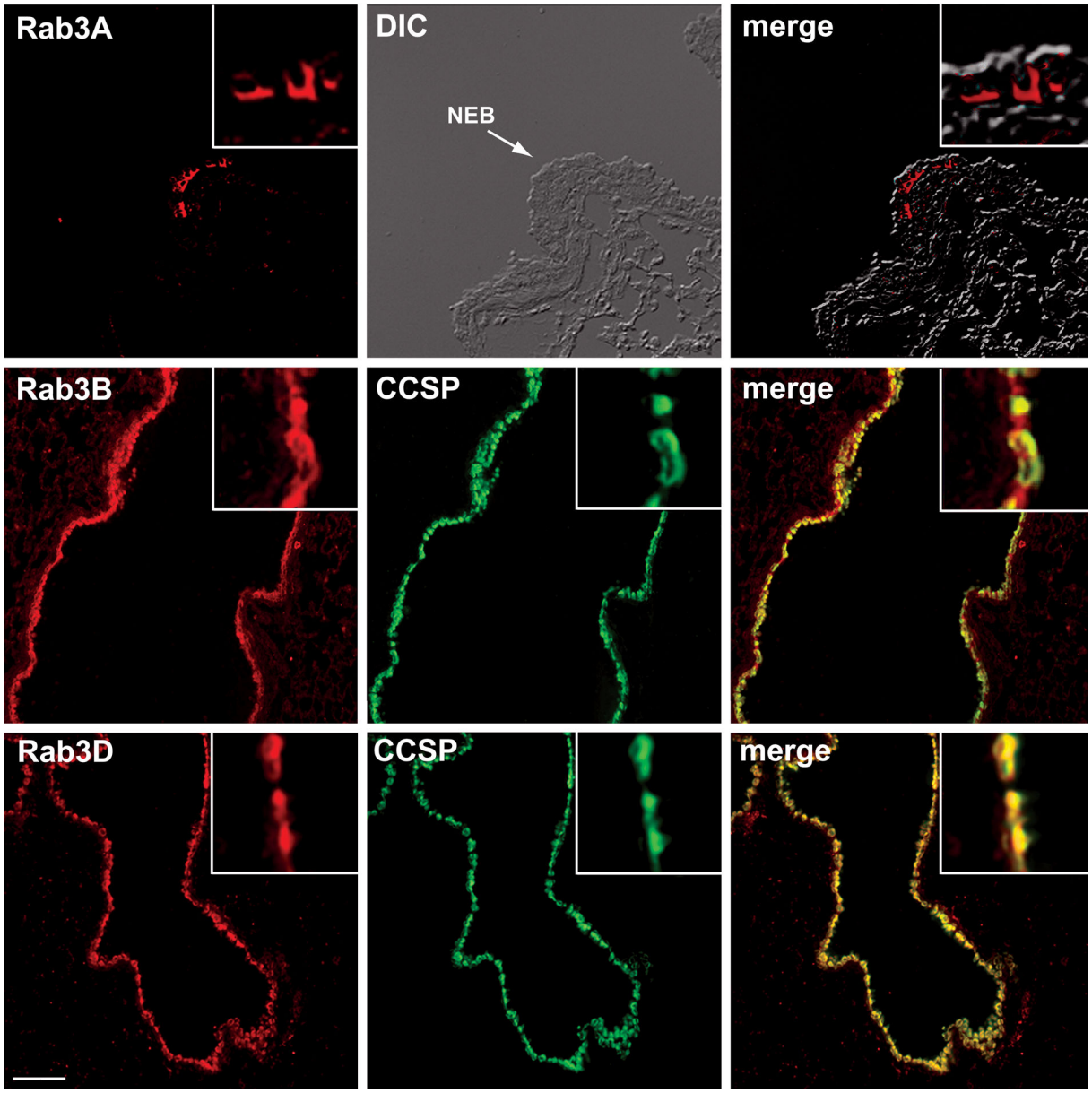

Figure 6.

Clara cells express components of the regulated exocytic machinery. Airways from unchallenged mice were labeled immunohistochemically for expression of Rab3 isoforms (red) and for CCSP (green). ***Top.*** Rab3A (red) localizes to the basolateral surfaces of the cells located in a neuroendocrine body (NEB). ***Middle.*** Rab3B in the bronchial airways localizes to CCSP expressing Clara cells (yellow in merged image) and is also found cells that do not contain CCSP (red in merged image). ***Bottom.*** In the bronchial airways, Rab3D is expressed only by Clara cells (yellow in merged image). Scale bar represents 50 μm (*top row*) and 100 μm (middle and bottom rows). Data are representative of experiments performed in 3 animals.

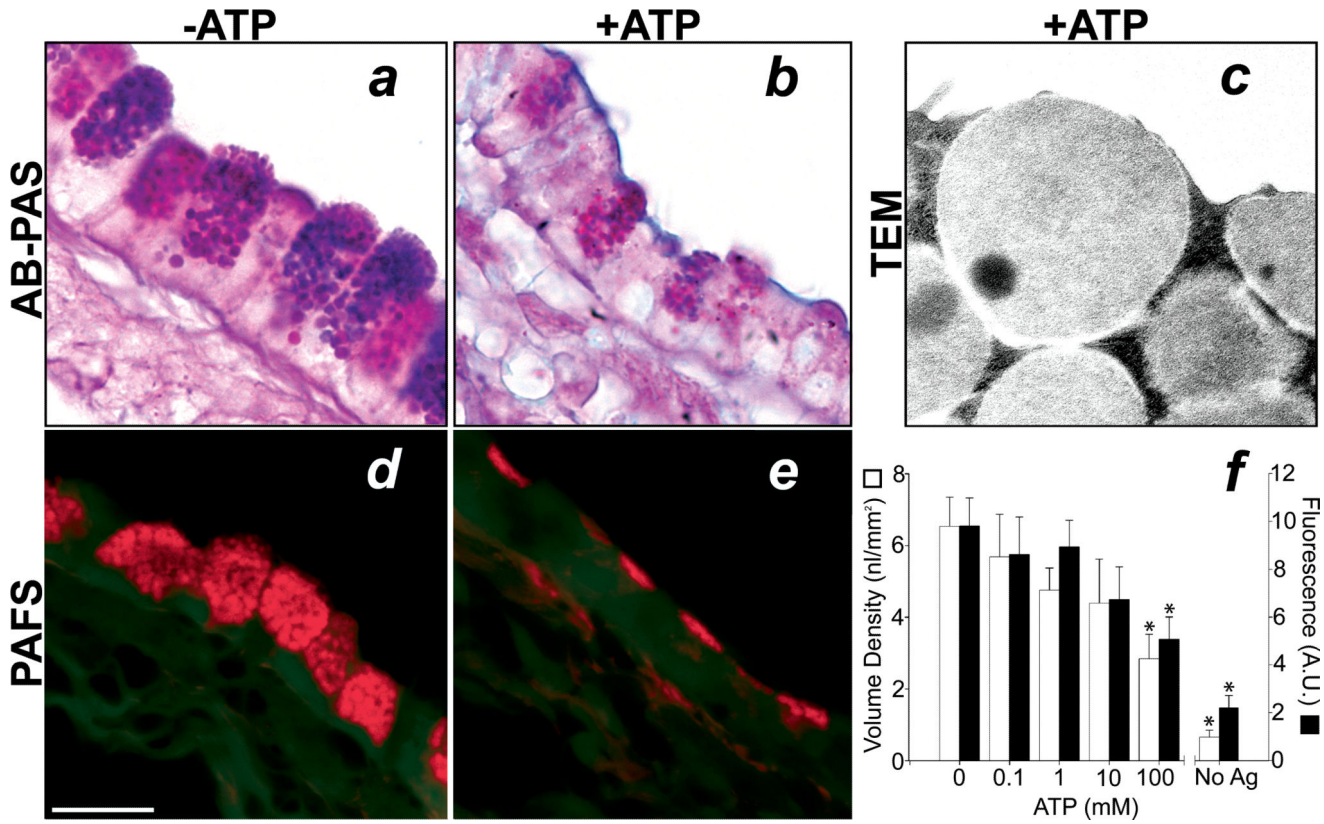

Figure 7.

Mucin is secreted from airway epithelial cells in a ligand-regulated manner. In mice 3 days after antigen exposure, increasing concentrations of aerosolized ATP (0.1–100 mM, 5 min) cause a dose dependent decrease in AB-PAS and PAFS staining. ***Top.*** In the absence of an ATP aerosol, mucous cells in antigen challenged mice contain large granular stores of AB-PAS positive mucin (*a*). Exposure of mice to ATP (100 mM, 5 min) causes an acute decrease in intracellular AB-PAS positive mucin stores (*b*). In mice euthanized immediately after ATP inhalation secretory granule fusion events are frequently observed (*c*). ***Bottom.*** The degree of ATP-induced secretion was measured in PAFS stained sections from antigen challenged mice that received aerosolized ATP (*d*) compared to animals that received aerosolized saline alone (*e*). The dose dependence of ATP-stimulated mucin secretion was quantified using volume density measurements (*open bars*) and fluorescence quantitation (*closed bars*) in PAFS stained sections (*f*). Scale bar is 10 μm in *a*, *b*, *d*, and *e* and 250 nm in *c*. * indicates statistically significant difference from antigen challenged mice not treated with ATP aerosol. Data from unchallenged mice are the same as in figure 4 (note different scale).

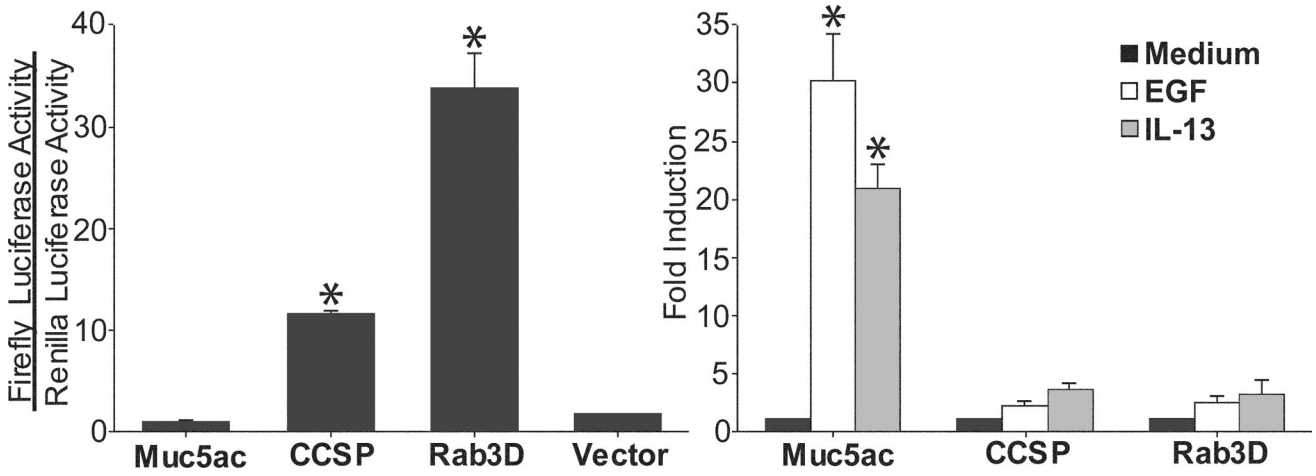

Figure 8.

Cytokine induction of secretory genes in Clara cells. Reporter constructs containing the firefly luciferase cDNA under the control of either the mouse Muc5ac, CCSP, or Rab3D promoters were co-transfected into mtCC1–2 cells with the HSV-TK Renilla luciferase control vector. ***Left.*** The CCSP and Rab3D promoters, but not the Muc5ac promoter or the promoterless firefly luciferase vector (pGL3 Basic), are constitutively active under resting conditions. * indicates statistically significant difference from Muc5ac and pGL3 Basic transfected cells. ***Right.*** Stimulation of mtCC1–2 cells for 24 h with IL-13 (100 ng/ml) or EGF (100 ng/ml) induces Muc5ac promoter activation. * indicates statistically significant difference from unstimulated Muc5ac promoter transfected cells.

Table 1.

Distribution of airways epithelial cell types in antigen challenged mice.

	Unchall.	6 Hours	1 Day	2 Days	3 Days	7 Days	14 Days	21 Days	28 Days	90 Days
Airway Cell Types										
Total No. Cells/mm	175 ± 24	177 ± 11	195 ± 14	177 ± 20	205 ± 14	176 ± 12	183 ± 10	216 ± 27	171 ± 11	192 ± 7
% Total										
Clara	54 ± 5	57 ± 6	54 ± 2	61 ± 7	58 ± 3	54 ± 2	60 ± 2	58 ± 7	55 ± 3	50 ± 2
Ciliated	43 ± 7	42 ± 0.3	43 ± 17	36 ± 2	41 ± 4	45 ± 4	40 ± 4	41 ± 5	44 ± 4	49 ± 1
Indeterminate	2.5 ± 2	0.5 ± 0.5	2.4 ± 1.2	3.4 ± 1.3	1.1 ± 0.3	1.2 ± 0.6	0.5 ± 0.3	0.7 ± 0.4	0.1 ± 0.1	1.4 ± 0.8
Proliferating Cells										
Total No. Cells/mm	1.1 ± 0.8	ND	0.1 ± 0.1	4.4 ± 2.7	4.2 ± 2.1	0.8 ± 0.5	0.6 ± 0.4	0.8 ± 0.2	ND	ND
% Total Cells	0.6 ± 0.4	ND	.05 ± .05	2.5 ± 1.5	2.0 ± 1.0	0.4 ± 0.3	0.3 ± 0.2	0.4 ± 0.1	ND	ND

Data are presented as mean number or percentage of cells per mm basement membrane ± SEM

ND, None Detected